Desalination 604 (2025) 118722

Contents lists available at ScienceDirect

Desalination

journal homepage: www.elsevier.com/locate/desal

Metal-organic frameworks/graphene oxide nanohybrids to control pore wetting in membrane distillation

Andoni Moriones [a,b,1], Lucía Cano-Herranz [a,b,1], Jose Miguel Luque-Alled [a,b,*], Carlos Téllez [a,b], Patricia Gorgojo [a,b,c,**]

[a] Instituto de Nanociencia y Materiales de Aragón (INMA) CSIC-Universidad de Zaragoza, Zaragoza 50018, Spain
[b] Departamento de Ingeniería Química y Tecnologías del Medio Ambiente, Universidad de Zaragoza, Zaragoza 50009, Spain
[c] Department of Chemical Engineering, Faculty of Science and Engineering, The University of Manchester, Manchester M13 9PL, United Kingdom

HIGHLIGHTS

- Metal-organic frameworks-graphene oxide nanohybrids were synthesised.
- The incorporation of nanohybrids delayed pore-wetting in membrane distillation.
- Control membrane showed adequate salt rejection for 4.5 h.
- Nanohybrid membranes maintaied very high salt rejection over 100 h.
- Adsorption properties of metal-organic frameworks were key to prevent membrane failure.

GRAPHICAL ABSTRACT

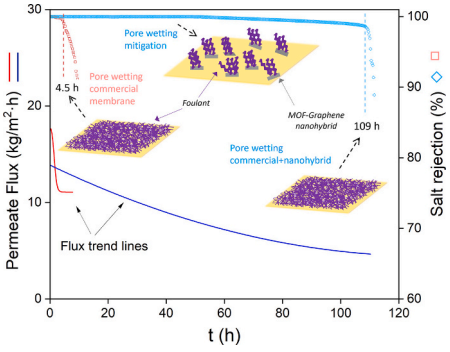

ARTICLE INFO

Keywords:
Membrane distillation
Graphene oxide
Zeolitic imidazole frameworks
UiO-66
Nanoadsorbents
Desalination

ABSTRACT

Membrane distillation (MD) is an emerging technology in the field of water desalination due to its high-energy efficiency and the fact that is not affected by feed salt concentration. As an alternative to feed water pretreatment, membrane surface modification aims at changing different properties to make it less prone to fouling. This work addresses the mitigation of the most concerning membrane degradation effects in MD, such as pore wetting and fouling, by modifying the membrane surface. This work takes advantage of the adsorption properties of metal-organic frameworks (MOF)@graphene oxide (GO) nanohybrids to create sacrificial sites (located zones where adsorption of foulants is facilitated) on the membrane surface. MOF@GO nanohybrids are embedded between two polydopamine (PDA) layers that are deposited on top of commercial polyethylene (PE) membranes. Two types of MOF@GO nanohybrids were evaluated, one containing UiO-66-NH_2 and the other one ZIF-8. Air gap membrane distillation (AGMD) experiments using highly concentrated foulant solutions to accelerate the effects of membrane degradation, showed that surface modification effectively extended membrane life. The selective foulant adsorption delayed pore wetting and allowed to retain most of the membrane flux. Pore wetting occurred after 109 h for the membrane containing ZIF-8@GO (500 mg·m^{-2}), compared to 4–5

* Correspondence to: J.M. Luque-Alled, Departamento de Ingeniería Química y Tecnologías del Medio Ambiente, Universidad de Zaragoza, Zaragoza 50009, Spain.
** Correspondence to: P. Gorgojo, Instituto de Nanociencia y Materiales de Aragón (INMA) CSIC-Universidad de Zaragoza, Zaragoza 50018, Spain.
E-mail addresses: jose.luque@unizar.es (J.M. Luque-Alled), pgorgojo@unizar.es (P. Gorgojo).
[1] Both authors contributed equally to this work.

https://doi.org/10.1016/j.desal.2025.118722
Received 15 November 2024; Received in revised form 12 February 2025; Accepted 18 February 2025
Available online 19 February 2025

h for the unmodified commercial membrane. Due to their high adsorption properties, the presence of MOFs is essential to ensure the formation of sacrificial sites and to maintain the initial flux, thus higher fluxes were observed for MOF@GO membranes (13 $kg{\cdot}m^{-2}{\cdot}h^{-1}$), compared to those containing only GO (5 $kg{\cdot}m^{-2}{\cdot}h^{-1}$).

1. Introduction

Access to safe drinking water is one of the biggest global challenges today. Current population growth, geopolitical conflicts, and the adverse effects of climate change have led to increasing water scarcity and stress. Moreover, increased water consumption results in a higher volume of wastewater that requires treatment before being reused or discharged into watercourses and natural resources [1]. It is estimated that only about 11 % of all domestic and industrial wastewater worldwide is reused [2]. Therefore, there is an urgent need to develop more energy-efficient separation methods for both drinking water and wastewater. Furthermore, it is important to note that only 1 % of the Earth's water is considered usable or accessible freshwater, with the majority being surface water and groundwater [3]. Desalination of sea and ocean water is a viable alternative for countries and regions with access to these resources [4,5]. Membrane separation processes, particularly reverse osmosis (RO), dominate the world market for desalination technologies [5]. However, in recent years, certain technologies have emerged as alternatives [3]. Membrane distillation (MD) is a thermally driven process that does not require overcoming osmotic pressure. The use of a hydrophobic membrane, combined with a vapour pressure difference between the feed and permeate sides, allows water molecules to pass in the vapour phase while blocking the passage of salts, and other non-volatile compounds and contaminants dissolved in the water. Thus, the high selectivity is a result of the vaporization process, resulting in very high separation efficiencies and salt rejections. MD has several advantages over RO, which include the ability to handle high feed salinities [6,7], higher resistance to fouling due to lower pressure requirements [7,8], and the allowance for energy reintegration [6,9]. However, the main challenge of this technology is obtaining high permeate fluxes and increasing energy efficiency [10]. In recent years, energy consumption in MD-based desalination processes has been significantly reduced through various strategies, resulting in lower specific costs. Advancements in utilizing waste heat and implementing heat recovery systems have significantly reduced the cost of desalinated water from MD plants, making them competitive with conventional reverse osmosis (RO) plants, which have a similar estimated cost per cubic meter of water produced [9,11,12].

As abovementioned, MD is able to operate in the presence of elevated salinity levels in the feed stream. Thus, this technology is particularly useful for treating water with high salt concentrations, such as seawater or brines from the agri-food [13], textile [14], and pharmaceutical industries [15]. In industrial environments, it is important to sustain a consistent flow rate over extended periods of time, without being affected by water contaminants such as salts, heavy metals, and organic matter. To achieve this, it is crucial to maintain a clean membrane surface free of fouling layers and pore-blocking substances to ensure stable performance [7]. In the case of MD, the fouling layer is hydrated, which means that the evaporating water molecules are not necessarily physically obstructed by this layer. However, it can lower the temperature at the vapour-liquid interface, reducing the driving force for vapour transport and ultimately decreasing the permeate flux [16]. Unlike pressure-driven reverse osmosis (RO) processes, in MD, rejection is directly affected by fouling on the membrane surface due to the phenomenon of pore wetting [7]. Pore wetting occurs when substances and particles accumulate on the membrane surface and on the pore walls, creating a hydrophilic bridge that allows liquid phase molecules to pass through the membrane. Pore wetting can be superficial, partial or total [17]. This phenomenon is critical in long-term operations, as it significantly reduces rejection and contaminates the permeate tank, thereby shortening the lifespan of the membrane and limiting its industrial applications. To the best of our knowledge, membrane fouling and wetting mechanism is still not fully comprehended.

Various strategies can be employed to prevent fouling and pore wetting in MD. Pre-treatment of feed water before the MD stage is often necessary, but it can greatly increase maintenance costs and it eventually becomes ineffective [17,18]. An alternative to pre-treatment is modifying the membrane surface, for example, by adding nanomaterials to provide anti-fouling properties [19,20]. 2D materials, such as graphene and their derivatives, are ideal for this purpose due to their high surface area and surface area-to-volume ratio [19,21]. Graphene oxide (GO) is a graphene-like material containing oxygenated functional groups such as alcohol, epoxide, ketone, or carboxyl, which can be easily obtained by an inexpensive and scalable method using graphite as a starting material. In addition, the presence of functional groups increases the space between layers and enhance chemical reactivity, resulting in hydrophilic properties and the ability to be easily functionalized. GO has proven to exhibit anti-fouling properties in MD processes. Alberto et al. [21] fabricated a sandwich-like structure with GO flakes between two polydopamine layers, loaded it on a hydrophobic support, and tested it using a salt solution with a non-ionic surfactant (Triton X-100) for 70 h, guaranteeing salt retention of 99.9 %. Lu et al. [22] prepared n-butylamine-functionalized GO/Polyvinylidene fluoride (PVDF) mixed matrix membranes for seawater desalination using MD. Mechanical strength and pore wetting were improved when raising the nanomaterial loading. However, porosity decreased due to the higher viscosity of the casting solution, which ultimately caused flux reduction. Zahirifar et al. [23] coated a layer of octadecylamine functionalized GO on top of a PVDF support achieving stable desalination performance on MD for 5 days with 98 % rejection. In another study, Woo et al. [24] investigated the desalination performance of a graphene-loaded superhydrophobic electrospun nanofiber membrane. They reported that at a certain graphene concentration, the mixed matrix membrane morphology and permeation properties were significantly improved, achieving 22.9 L m^{-2} h^{-1} flux and 99.99 % rejection.

Metal-organic frameworks (MOFs) are hybrid porous materials formed by coordinating metal ions with organic ligands, generating crystalline networks of one, two, or three dimensions. The arrangement of metal atoms in their structure gives both MOFs thermal stability, up to temperatures of 300–400 °C, and chemical stability, being stable in water and organic solvents. MOFs are known for their strong adsorption capacity, which is attributed to their high specific surface and pore volume, tunable pore size, and facile functionalization. MOFs can act as nanoadsorbents, increasing the selectivity and efficiency of separation processes, and therefore are very attractive materials for improving many membrane applications [25,26]. There are various structures and types of MOFs. ZIFs (zeolitic imidazole frameworks) [27] and UiOs (named after the University of Oslo) [28] are two of the most extensively researched families, which have also been explored for MD applications [29,30]. Li et al. [31] prepared a Janus membrane by functionalizing polytetrafluoroethylene (PTFE) with different ratios of UiO-66-NH_2 and GO, reaching 48 h of stable flux with excellent rejection of 99.99 %. The formation of a hydrophilic layer over the hydrophobic PTFE was able to successfully delay pore wetting. However, the potential of hybrids formed by MOF grown on GO, instead of just a combination of individual components of both, has been barely investigated. To our knowledge, only MOF-801 has been grown in GO to be used in MD desalination processes, being its mission to achieve hydrophobic membranes that increase water flow [32]. MOF@GO hybrids exhibit strong interfacial bonding due to the anchoring of metal clusters to the functional groups

of GO. Zn^{2+} coordinate with carboxyl and epoxide groups, while the subsequent incorporation of ligand molecules facilitates the growth of the MOF on the basal plane of the nanosheet. Additionally, these linkages enhance the dispersibility of MOFs over the GO, effectively preventing agglomeration [33–35]. Similar MOF@GO hybrids have been explored for a broad range of applications, including anti-fouling properties in nanofiltration applications [36,37], showing excellent nanomaterial stability. Thus, the synthesis of MOFs onto the basal planes of GO enables the full exploitation of their adsorption and hydrophilic/hydrophobic properties, as they are homogenously dispersed and accessible to foulants.

This study aims to combine the adsorption capacity of MOFs and 2D graphene oxide flakes to mitigate fouling and control pore wetting in commercially available polyethylene (PE) membranes for MD applications. UiO-66-NH_2 and ZIF-8 are chosen to represent two of the most studied families of MOFs. UiO-66-NH_2 is a zirconium-based MOF belonging to the isoreticular series of UiO-66. This family of MOFs is well known for its hydrophilicity, and the addition of the amine group further improves this property. ZIF-8 is the best-known member of its family and its recognized for its high adsorption capacity and hydrophobic properties [38]. In this work, both MOFs are synthesized on the basal plane of GO in a one-step process to obtain ZIF-8@GO and UiO-66-NH_2@GO. Theses nanohybrid materials are then deposited on top of a commercial PE membrane with the aid of polydopamine (PDA). PDA is widely utilized for its adhesive properties, acting as a bridge between the polymer and nanohybrids. The use of two PDA coatings enables the effective retention of nanohybrids within its structure. Besides, PDA coating forms a mesh-like structure that allows the free transport of molecules, ensuring that the embedded nanohybrids remain accessible to water and foulant molecules. These membranes will be tested for air gap membrane distillation (AGMD) using a feed containing sodium chloride and high concentrations of organic and inorganic fouling agents. In addition, extensive characterization and MD tests under different conditions performed in this study help comprehend the interaction between foulant nature and membrane surface properties.

2. Experimental

2.1. Materials

Graphene oxide (GO, 1 wt%) was purchased from Williamblythe (UK). Dopamine hydrochloride (DA, ≥ 98 %), 2-methylimidazole (Hmim, ≥99 %), zinc nitrate hexahydrate ($Zn(NO_3)_2{\cdot}6H_2O$, ≥ 99 %), ammonium hydroxide (NH_4OH, 20.0–30.0 % NH_3 basis), humic acid (HA), sodium chloride (≥ 99.0 %) and Triton X – 100 were purchased from Sigma Aldrich (Germany). Tris (hydroxymethyl) aminomethane (TRIS) was purchased from AcrosOrganics (Belgium). Isopropyl alcohol (IPA, ≥ 99.5 %) was purchased from Honeywell (USA, ≥ 99.5 %). Polyethylene (PE) membranes were purchased from Aquastill (Netherlands) with a mean pore radius of 0.16 μm and average thickness of 113 μm. Zirconium tetrachloride ($ZrCl_4$, > 99.5 %) was purchased from Alfa Aesar (Spain). Aminoterephthalic acid (H_2N-H_2BDC, > 99 %) and formic acid (> 90 %) was purchased from Fischer Scientific (Spain). Ethanol (> 99.5 %) and deionized water (DI) were purchased from Gilca (Spain).

2.2. Synthesis of UiO-66-NH_2@GO nanohybrids

UiO-66-NH_2 was synthesized onto GO flakes, by dissolving first 466 mg of $ZrCl_4$ (2 mmol) in 30 mL of 1 wt% GO dispersion in water. This allowed electrostatic interactions between Zr(IV) cations and negatively charged functional groups in GO. Another solution was prepared by dissolving 179.13 mg H_2N-H_2BDC (1 mmol) in 20 mL of ethanol and 25 mL of formic acid 30 % $v{\cdot}v^{-1}$. Then both solutions were mixed turning into light brown-yellowish colour, and transferred to an autoclave, which was kept at 110 °C for 12 h. Finally, the product was washed three times with ethanol and twice with distilled water and dried at 60 °C for 12 h under vacuum. The same procedure was carried out without GO to obtain pure UiO-66-NH_2 crystals.

2.3. Synthesis of ZIF-8@GO nanohybrids

ZIF-8@GO nanohybrids were prepared by adding GO in the synthesis liquor prepared using the reagents and concentrations for ZIF-8 synthesis reported elsewhere [39]. Firstly, 0.594 g of zinc nitrate hexahydrate (2 mmol) were dissolved in 13 mL of 1 wt% GO dispersion in water to enable the coordination of Zn(II) to the basal plane of GO. Secondly, 0.328 g of Hmim (4 mmol) were dissolved in 3.76 g NH_4OH. Both solutions were mixed, turning into a greyish suspension, which was stirred for 10 min at room temperature to undergo crystallization. The product was then centrifuged and washed with deionized water at least 3 times and dried at 60 °C in a vacuum oven. The same procedure was carried out without GO to obtain pure ZIF-8 crystals.

2.4. Membrane preparation

Dopamine-functionalized PE membranes were prepared via facile surface coating following the procedure reported by Alberto et al. [21] The coating solution was prepared by dissolving DA in a TRIS-HCl buffer solution (10 mM, pH = 8.5) at a concentration of 2 $mg{\cdot}mL^{-1}$. The solution was stirred for 30 min to allow for the first stage of polymerization, which is more heterogeneous and could cause defects on the membrane surface [40]. Then, the PE membranes were floated in the DA solution for 2 h for subsequent self-polymerization, leading to a PDA layer coating the PE surface. The PDA-functionalized PE membranes (PDA/PE) were rinsed using deionized water and dried in a vacuum oven at 60 °C for 2 h. Once dried, the modified membranes were immersed in IPA for 30 min to activate the pores and allow their full wetting.

Dispersions of GO nanohybrids (either UiO-66-NH_2@GO or ZIF-8@GO) were prepared by adding the powder into 100 mL water/IPA mixtures (1:1 volume ratio), stirring for 10 min, sonicating for another 10 min and repeating the stirring and sonication process two times. Afterwards, the dispersions were vacuum filtered onto membrane discs of 44.2 cm^2, where the deposited amount of nanohybrids ranged from 100 to 1000 mg per m^2 of membrane. The membranes were dried in a vacuum oven at 60 °C for 2 h, and another PDA layer was added on top following the same procedure as for the first PDA layer (Fig. 1) to immobilize the GO derivative. A more detailed schematic of the

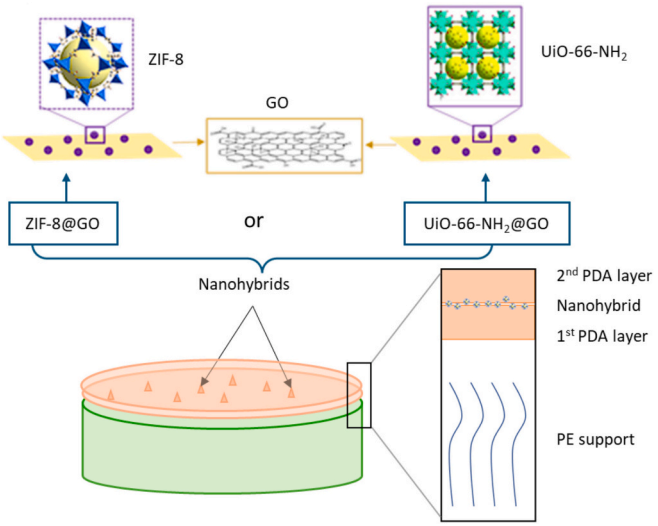

Fig. 1. Scheme of the membrane structure including an illustration of the chemical structure of the nanoadsorbents.

fabrication process is shown in Fig. S1.

PDA-functionalized PE membranes (without nanohybrids) were also prepared for comparison. Synthesized membranes and their characteristics are shown in Table 1. The loading *(L)* of the nanohybrids was calculated dividing the amount of the MOF@GO deposited *(m)* divided by the membrane area *(A)* (See Eq. 1). Where *m* is the product of dispersion concentration *(C)* and volume *(V)* (See Eq. 2):

$$L = m \cdot A^{-1} \tag{1}$$

$$m = C \cdot V \tag{2}$$

2.5. Air gap membrane distillation (AGMD) tests

Air gap membrane distillation (AGMD) experiments were carried out in an in-house built system (a schematic representation is shown in Fig. 2). The air gap configuration was chosen due to its energy efficiency, simplicity, ease of operation and higher flux as compared to direct contact mode [41]. The feed solution was continuously stirring at 350 rpm and kept at 70 °C by using a hot plate with a thermocouple attached (IKA RCT standard 2.0). The feed was recirculated at 600 mL·min^{-1} using a 12 V pump. The condenser plate in contact with the permeate was cooled by a recirculating water flow (600 mL·min^{-1}) in counter current configuration coming from a chiller (Julabo F32) set at 2 °C. The membrane cell is made of acrylic plastic and had an effective area of 7.07 cm^2 and a 3 mm air gap. The system was also composed of a conductimeter (Cond60 VioLab) and a precision balance (Sartorius Practum 1102-1S) connected to a computer for real time data acquisition. The water vapour travelled through the hydrophobic pores from hot to cold side due to the vapour pressure across the membrane. The feed conductivity was measured at the beginning and at the end for every experiment to reassure that the feed tank did not suffer a noticeable change in salinity and driving force was kept almost constant during the process.

Aqueous feed solutions containing sodium chloride (35 g·L^{-1}), HA (500 ppm) and calcium chloride (420 ppm) were used. These components are representative of typical fouling agents [42,43], therefore chosen to study the anti-fouling and stability properties of the membranes under harsh conditions and accelerated fouling [44]. The pH of the feed was maintained ~7.5, simulating seawater [45].

The membrane performance was evaluated by continuous measurement of permeate flux and rejection. Flux (J (kg·m^{-2}·h^{-1})) was calculated as the permeate mass increment (Δm) in time (Δt) divided by the membrane effective area (A). See Eq. 3:

$$J\left(kg \cdot m^{-2} \cdot h^{-1}\right) = \Delta m \cdot A^{-1} \cdot \Delta t^{-1} \tag{3}$$

The rejection rate (R) was determined monitoring conductivity changes in the collected permeate (C_p) divided by the feed conductivity (C_f). See Eq. 4:

$$R\ (\%) = \left(C_f - C_p\right) \cdot C_f^{-1} \cdot 100 \tag{4}$$

The reported values of membrane flux and rejection correspond to a continuous measurement of these parameters. To ensure reproducibility, they were repeated two or three times, except for the long-term operation experiments (i.e. up to 120 h) that were performed only once.

Table 1
Membrane codes and their main specifications according to fabrication method. All membranes were prepared using PDA-coated PE and an additional PDA layer was formed after deposition of the nanoadsorbents.

Code	Type of nanohybrid	Loading (mg·m^{-2})
PE (as received)	–	–
PDA/PE	–	–
GO 50-PDA/PE		50
GO 75-PDA/PE		75
GO 100-PDA/PE	GO	100
GO 500-PDA/PE		500
GO 1000-PDA/PE		1000
U-G 100-PDA/PE		100
U-G 500-PDA/PE	UiO-66-NH_2@GO	500
U-G 1000-PDA/PE		1000
Z-G 100-PDA/PE		100
Z-G 500-PDA/PE	ZIF-8@GO	500
Z-G 1000-PDA/PE		1000

2.6. Nanohybrids characterization

X-ray diffraction analysis (XRD, PANalytical Empyrean X ray diffractometer) was used to determine the crystalline structure and purity of the synthesized materials. Data was registered in a 2θ range of 5–40° employing a Cu anode ($Cu_{k\alpha}$ $\lambda = 1.54186$ Å) with a voltage of 40 kV and a current of 40 mA as X-ray source. Scanning electron microscopy (SEM) coupled with an energy dispersive X-ray (EDX) was used to analyze particle size and growth of MOFs over GO sheets using a Field Emission F50 Inspect operating at 10 kV. Particle size distribution was calculated using the open-source software ImageJ® and estimated as the average of 100 measurements for each nanomaterial. Thermogravimetric analysis (TGA) was used to analyze thermal stability and nanohybrids composition by employing a Mettler Toledo TGA/SDTA 851e. These experiments were carried out from 35 to 700 °C under air atmosphere with flowrate of 100 mL (STP) ·min^{-1} at a heating rate of 10 °C·min^{-1}. Surface area was measured by nitrogen sorption analysis and BET method (Micromeritics Tristar 3000). X-ray photoelectron spectroscopy (XPS) analysis was conducted to study chemical compositions using a Kratos Axis Ultra spectrometer with a monochromatic Al Kα (1486.6 eV) X-ray source (10 mA, 15 kV and a power of 150 W) and data were analyzed using a CASAXPS software. For the determination of the HA adsorption capacity of nanofillers, different HA solutions with concentrations ranging from 10 to 200 mg·L^{-1} were prepared. After that, 20 mg of nanohybrid were added to these solutions and kept stirring at an orbital shaker for at least 24 h to allow HA adsorption. The solutions were then centrifuged at 9500 rpm during 45 min and filtrated with a syringe filter of 0.22 μm twice. The amount of free HA was quantified using a UV–Vis and a calibration curve at 254 nm. Then, the amount of HA adsorbed was calculated by the difference between the initial value and that in the mother liquor.

2.7. Membrane characterization

SEM-EDX (Field Emission F50 Inspect, 10 kV) was used to study the morphology and surface structure of pristine PE and PDA-functionalized PE. Water contact angle (WCA) was used to determine changes in membrane hydrophobicity by using a Krüss Shape Analyzer 10 MK2. Surface roughness was analyzed by atomic force microscopy (AFM) using a Bruker Multimode V AFM System, exchangeable scanner type J (200 μm(X) x 200 μm(Y) x 5 μm (Z), RTESPA-150, 5 N·m^{-1} symmetric tip, Al Reflex Coating)). Immobilization of the nanohybrids on top of the PDA/PE surface was investigated over time. The membranes were mounted inside the MD module and DI water was recirculated for 24 to 48 h. After this period, the DI water was examined using a V-670 Jasco UV–Vis spectrophotometer to identify the presence of nanohybrids or PDA in the water.

3. Results and discussion

3.1. Nanohybrids characterization

XRD analysis was performed on the nanohybrids to confirm the formation of the MOFs and crystalline phases of both UiO-66-NH_2 (Fig. 3a) and ZIF-8 (Fig. 3b). Their spectra are shown together with that of GO and pure MOFs, and were compared with simulated CIF files from the International Zeolite Association (IZA) database [46]. The

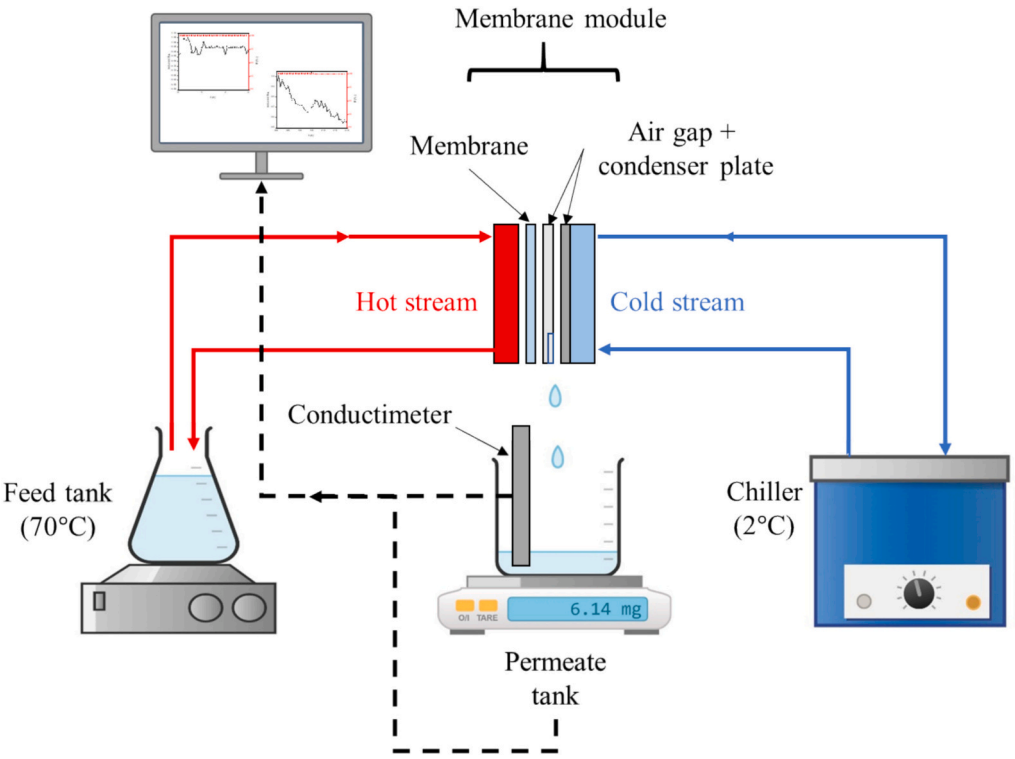

Fig. 2. Representation of the homemade AGMD distillation set up.

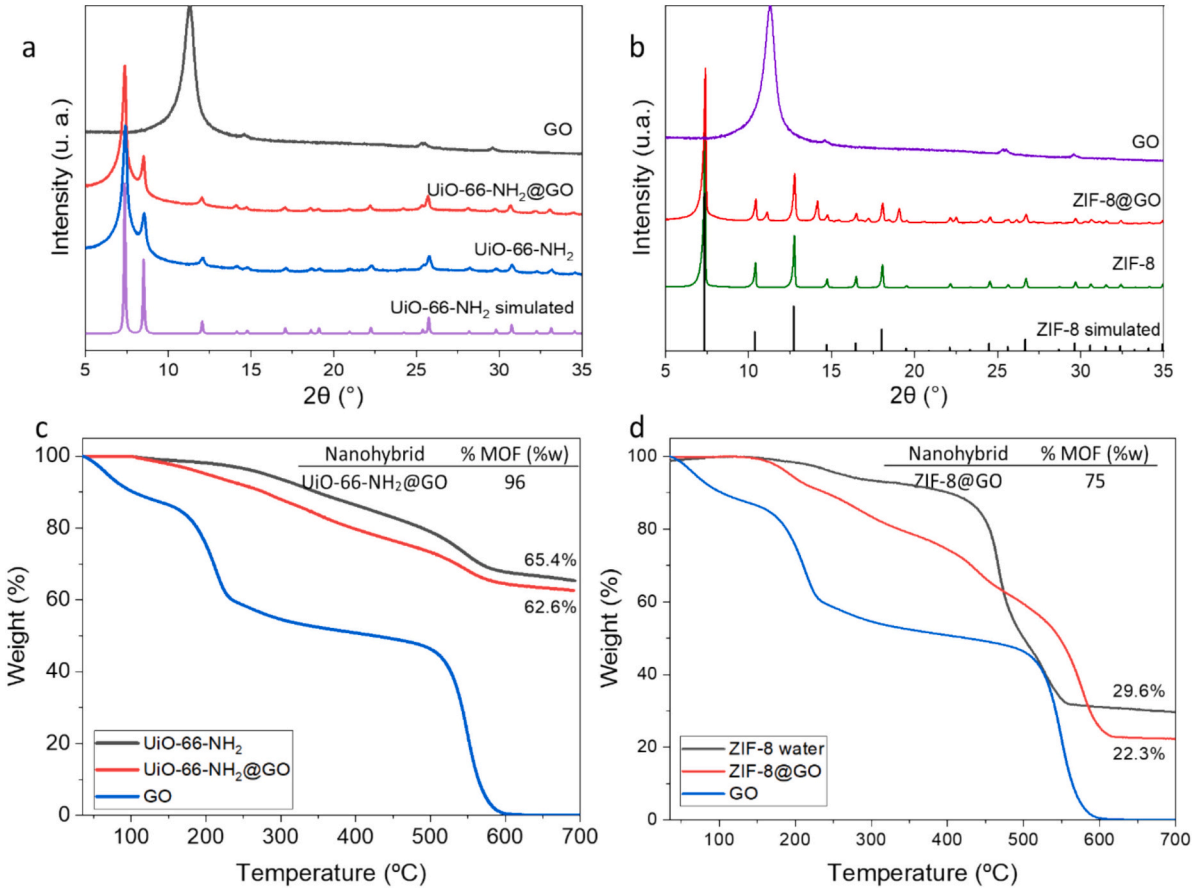

Fig. 3. XRD spectra (a and b) and TGA curves (c and d) for both UiO-66-NH_2@GO (a and c) and ZIF-8@GO (b and d) nanohybrids. XRD spectra and TGA curves of GO, UiO-66-NH_2 and ZIF-8 are plotted for comparison.

diffraction pattern of the GO shows a diffraction peak at around 11.2°, which is attributed to the interlaminar distance due to stacking of the 2D flakes [27]. This signal does not appear in the spectra of the nanohybrids due to the random stacking of the GO flakes resulting from the deposition of the MOFs [47]. The MOFs synthesized without GO match the simulated XRD pattern. The main diffraction peaks of both UiO-NH_2 and ZIF-8 are also found in their respective nanohybrid. The XRD spectrum of ZIF-8@GO contains additional small peaks that can be related to zinc hydroxide nitrate impurities (the peak at $2\theta = 11°$ could be related to Zn $(OH)(NO_3)(H_2O)$), in accordance with that observed by other authors. This by-product can be produced at very low quantities at low Hmim/Zn ratios, such as the one used here [47,48].

In order to calculate the MOF/GO ratio for the synthesized nanohybrids, thermogravimetric analysis was carried out. Fig. 3c and d displays the TGA curves from for UiO-66-NH_2@GO and ZIF-8@GO, respectively, together with that of GO and pure MOFs. The thermal degradation of GO occurs mainly in three stages. Up to 100 °C, superficially adsorbed water molecules are removed. Subsequently, two marked weight losses are observed due to the degradation of structural components: (i) 100 °C–360 °C, the removal of oxygen functional groups, and (ii) from 360 °C onwards, the oxidative pyrolysis of carbon structure [49]. Both ZIF-8 and UiO-66-NH_2, and their respective nanohybrids do not display weight loss up to 100 °C, probably due to the lower hydrophilicity as compared to bare GO. For UiO-66-NH_2, two weight losses are clearly distinguished. Between 100° and 400 °C, a weight loss of 14 % occurs due to dehydroxilation. Above this point, a 20 % weight loss step is be observed due to material decomposition [50]. ZIF-8 quickly collapses above 450 °C due to thermal decomposition of 2-MeIm, which leads to the formation of ZnO as the final calcination product [51]. However, the weight loss in both nanohybrids (UiO-66-NH_2@GO and ZIF-8@GO) follows a constant pace due to the degradation of structural moieties in GO and MOFs. MOF/GO ratios were calculated considering that GO degrades completely at 700 °C while that the remaining weight for both nanohybrids were 62.6 % for UiO-66-NH_2@GO and 22.3 % for ZIF-8@GO (see Fig. 3c and d). By comparing this remaining weight with that of the pure MOF, UiO-66-NH_2 (65.4 %) and ZIF-8 (29.6 %) samples, the percentage of the MOF in the nanohybrids can be calculated. The obtained compositions, 95.7 wt% MOF in UiO-66-NH_2@GO and 75.3 wt% MOF in ZIF-8@GO, are shown in an inset along with the weight loss curves.

Morphology and particle size of all materials were estimated using SEM. For the synthesis of pure MOFs (Fig. 4a and b), nanoparticles of 719 (±113) and 130 (±4) nm were observed for ZIF-8 [39] and UiO-66-NH_2 [52], respectively. Fig. 4c and d show the SEM images of the nanohybrids, UiO-66-NH_2@GO and ZIF-8@GO, respectively. The 2D flakes correspond to the GO and the nanoparticles on top of them evidence the presence of MOFs (UiO-66-NH_2 in Fig. 4c, and ZIF-8 in Fig. 4d). The commercial GO flakes have a wide and heterogeneous size distribution, ranging from a lateral size of 5 up to 30 μm and a thickness of 2 nm, as granted by seller. This size makes it suitable for the deposition onto the PE support (pore radius of 0.16 μm). Fig. 4c shows the presence of several UiO-66-NH_2 nanoparticles homogenously grown on the surface of the GO flakes, although they partially lost their characteristic cubic morphology. The observed change in shape agrees with previously reported results [53,54]. ZIF-8 nanoparticles, on the contrary, grew with their distinct cubic shape [27,55], unaltered by the presence of GO, and were also homogenously distributed along the GO basal plane without agglomerating (see Fig. 4d). The nanoparticles grown on top of the GO had an average particle size of 132 (±3) and 746 (±11) nm for UiO-66-NH_2@GO and ZIF-8@GO, respectively. Fig. S2 displays the particle size distributions for pure MOFs and both nanohybrids.

N_2 adsorption-desorption experiments were carried out to obtain the BET surface area of the synthesized nanomaterials. The isotherms are shown in Fig. S4 and all samples exhibited type I isotherms according to the IUPAC classification. Both nanohybrids show a certain presence of mesopores at high values of P/P_0, which can be related to voids between the particles. Both UiO-66-NH_2 and ZIF-8 (928 and 1059 $m^2 \cdot g^{-1}$, respectively) showed higher specific surface areas that their corresponding counterparts synthesized over GO flakes. This is believed to be related to the contribution of non-porous GO (which exhibits minimal N_2 adsorption, at approximately 2 m^2/g [56,57]) and the pore blocking of MOFs due to poor accessibility of stacked 2D flakes [58]. The reduction was estimated to be 45 % for UiO-66-NH_2@GO (512 $m^2 \cdot g^{-1}$) and 82 % for ZIF-8@GO (194 $m^2 \cdot g^{-1}$).

3.2. Membrane characterization

SEM images of the membranes were acquired after each of the three modification steps to observe changes in morphology throughout the process (Fig. 5). It should be noted that the samples employed for the SEM analysis (PDA/PE, UiO-66-NH_2@GO/PDA/PE, and ZIF-8@GO/PDA/PE) contain a single PDA layer, which differs from the membranes presented in Table 1 (dual PDA layer configuration in a layered structure as depicted in Fig. 1). In other words, the second PDA coating (after nanohybrid deposition) was not applied to the SEM samples with the aim of avoiding any potential interference from the covering layer. Therefore, samples in Fig. 5 do not follow the coding shown in Table 1. Fig. 5a corresponds to the bare polymeric support, in which some pores were identified (indicated with red circles). After the formation of the first PDA layer (Fig. 5b), pores and fibre gaps seem to be partially covered, with an increase in the surface roughness as compared to the original PE membrane (304 vs 288 RMS value, see Fig. S4). SEM images in Fig. 5c and d correspond to the membrane surface modified with one layer of PDA and nanohybrids. The presence of these nanohybrids on top of the PDA/PE layers is confirmed; i.e. UiO-66-NH_2@GO/PDA/PE (Fig. 5c) and ZIF-8@GO/PDA/PE (Fig. 5d). In addition, it can be observed that MOF nanoparticles on top of GO maintained their original structure and size after membrane fabrication. SEM images of a control membrane containing two PDA layers over the PE support were also taken. Results can be seen in Fig. S3, and show not noticeable change in membrane surface morphology or shape.

AFM measurements (Fig. S5) indicate that the nanohybrid deposition increased the membrane surface roughness. Ra and RMS parameters (288 and 236.8 nm for PE) raised by 97 % and 75 %, respectively (509 and 416 nm) for the U-G 500-PDA/PE membrane.

High Resolution SEM (HR-SEM) images were taken in order to check the structure and different layers that comprise the membrane. As can be seen in Fig. S6, membrane contains two different regions, the PE support behind (highlighted by the green arrow) and the surface, consisting of two PDA layers with the hybrid in between (highlighted by the yellow arrow) with a thickness of around 0.3 μm.

WCA was performed to examine the hydrophobic properties of the membranes (Fig. 6a). For the bare polymer after the addition of two PDA layers without nanomaterial, wettability increased (i.e. decreased WCA) due to the hydrophilicity of this polymer. Besides, the increase in roughness (confirmed by AFM, Fig. S5) also contributes to decrease WCA values according to Wenzel and Cassie Baxter equations (see Eq. S1), which states that the observed WCA is directly proportional to the cosine of the actual WCA. In other words, the surface roughness amplifies surface hydrophilicity or hydrophobicity [59,60]. For the UiO-66-NH_2@GO membranes, despite the presence of hydrophilic groups in the nanohybrids, the WCA of the modified membranes increases with the loading (100, 500, and 1000 $mg \cdot m^2$). The same tendencies have already been reported for other authors and it is believed to be related to the presence of hydrophobic regions in GO, therefore weakening the effect of the hydrophilic MOF [8,61]. For membranes containing ZIF-8@GO nanohybrids, the WCA are higher PDA/PE and UiO-66-NH_2@GO membranes due to higher hydrophobic nature of ZIF-8.

High resolution XPS spectra of the C 1 s core level region for the membrane surface after every modification step is shown in Fig. 6b-d. As compared to PE (Fig. 6b), the concentration of C—C bonds decreases

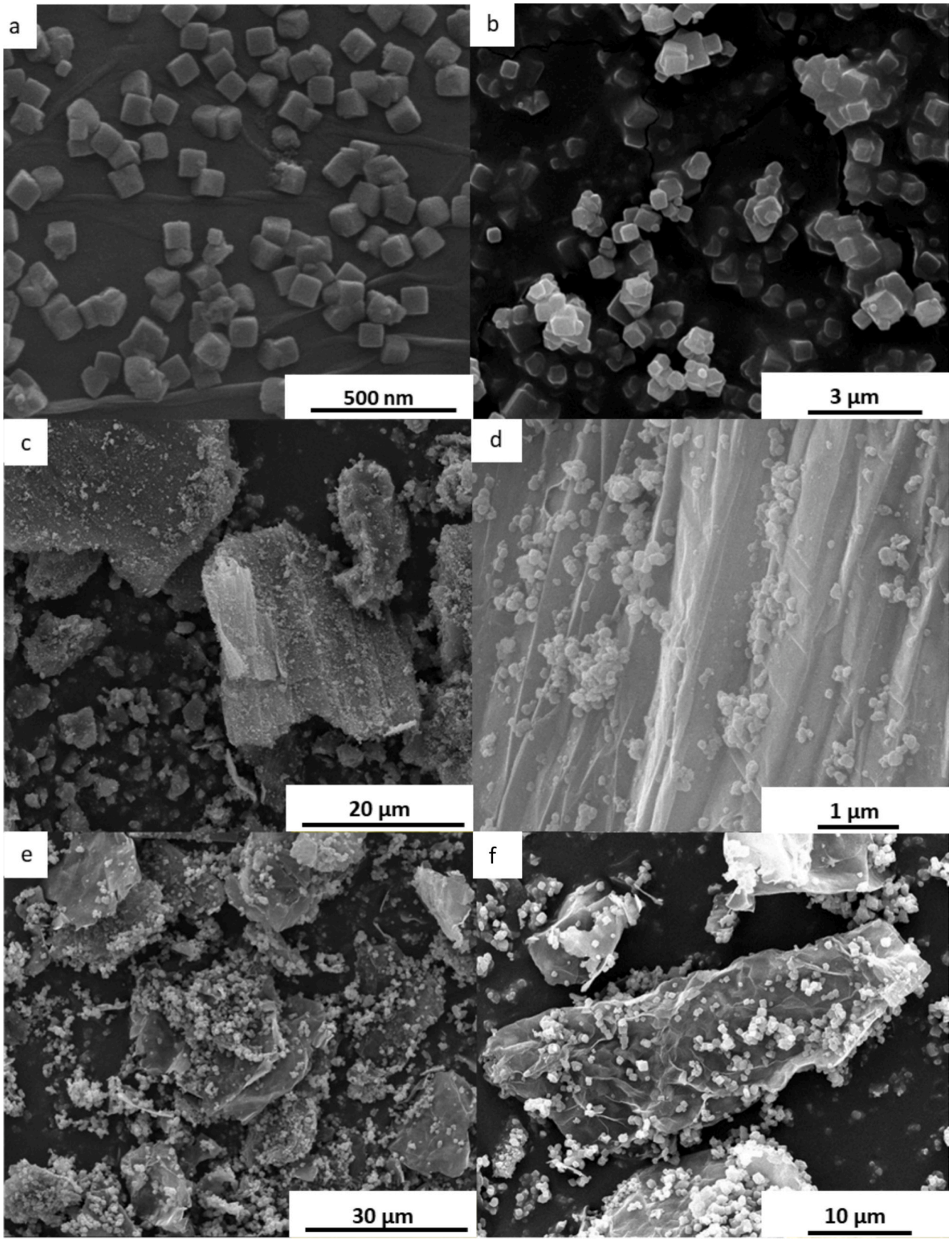

Fig. 4. SEM images of UiO-66-NH_2 (a) nanoparticles, ZIF-8 (b) nanoparticles, UiO-66-NH_2@GO (c-d), and ZIF-8@GO (e-f) nanohybrids.

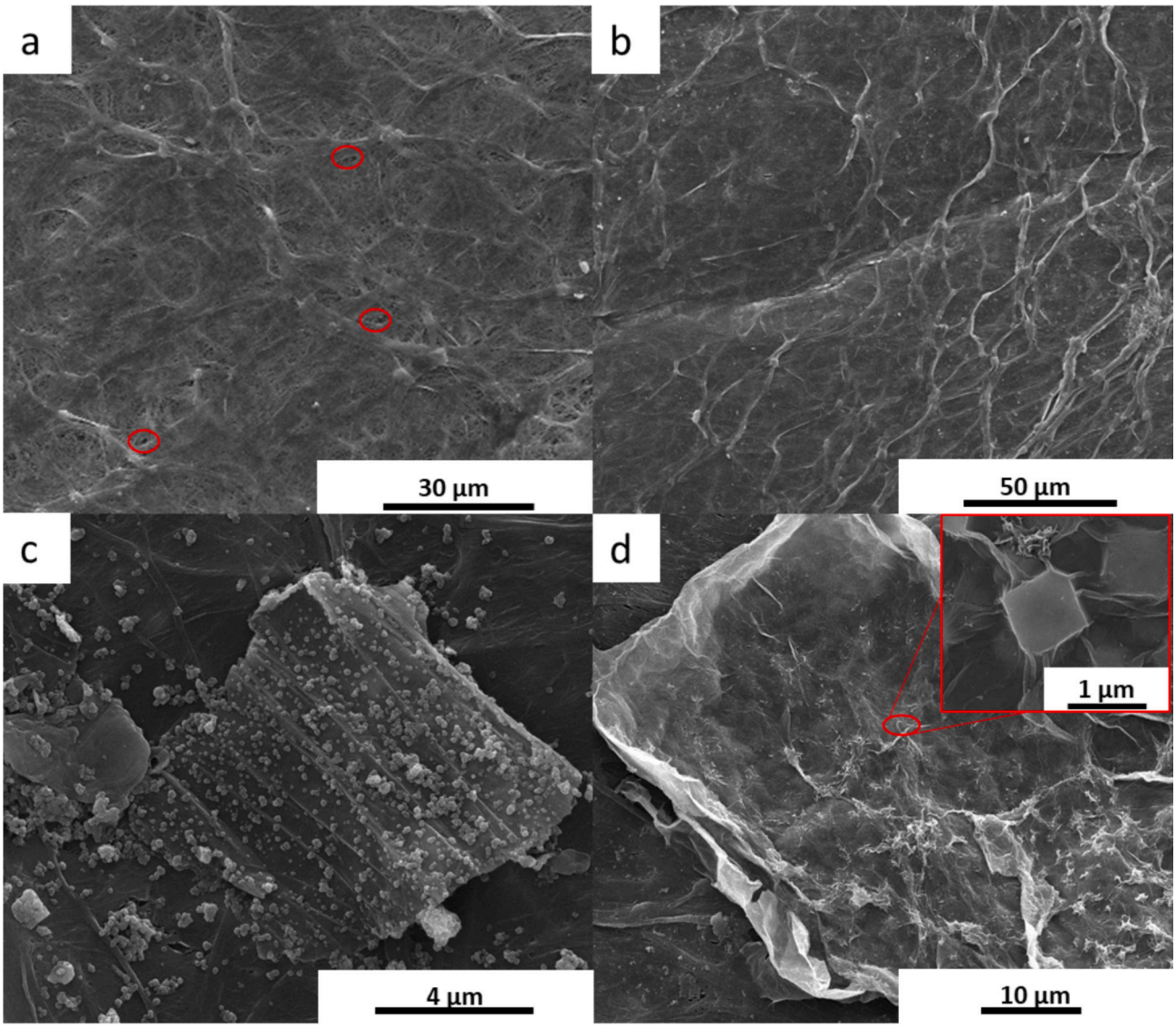

Fig. 5. SEM images of pristine PE membrane (a), PDA/PE (b), UiO-66-NH_2@GO/PDA/PE (c) and PDA/ZIF-8@GO/PDA/PE (d).

during the subsequent steps of membrane fabrication due to the contribution of other species. Both PDA/PE (Fig. 6c) and *Z*-G 500 PDA/PE (Fig. 6d) showed C-O/C-N and C=O/C=N peaks, confirming the existence of a PDA layer and nanohybrid on top of the PE membrane. After deposition of the nanohybrid (Z-G 500 membrane, Fig. 6d), the concentration of C=C increases and the C-O/C-N decreases as compared to PDA/PE (Fig. 6c) due to the presence of the imidazole group and graphene aromatic regions. Fig. S7 show obtained XPS spectra for the O 1 s, N 1 s and Zn 2p. In the N 1 s region, after the addition of the nanohybrid, C=N-C bond gets more intense due to the nanohybrid presence (imidazole group). In O 1 s region, the arising of a new bond at B.E. of 533 eV, related to GO addition of the nanohybrid, is identified. In the case of Z-G 500-PDA/PE membrane, Zn is also present (Fig. S7e), suggesting the deposition of ZIF-8@GO nanohybrids on the membrane surface. Furthermore, atomic compositions were determined from the high-resolution spectra of each atom. Fig. S7f summarizes the atomic concentrations of these elements for the tested membranes.

The stability of the membranes, i.e. the potential detachment of nanohybrids or PDA from the PE membrane, was analyzed as previously described in the experimental section. As can be seen in Fig. S8, commercial PE membranes were found to release molecules that absorb signal within the UV–Vis range. These are believed to be membrane preserving agents that are physically adsorbed into the membrane pores and that are easily removed with hot water (Fig. S8a). The addition of the PDA layers decreases significantly the signal coming from the PE substrate (Fig. S8a). The stability of membranes with a single PDA layer and GO (loading of 50 $mg{\cdot}m^{-2}$) was evaluated and it was found that the longer the testing (24 vs. 48 h), the higher the degree of detachment (Fig. S8b). This indicates that some PDA molecules or GO are not completely stuck to the PE membrane and falls off the surface. When a second layer of PDA is deposited (Fig. S8c), the signal from the PDA/nanohybrid detachment is significantly reduced, meaning that the second PDA layer is essential to preserve the membrane structure and properties after the addition of nanohybrids. The membranes with the ZIF-8@GO nanohybrid hardly show any signal, which would indicate that this nanohybrid shows good stability after the second PDA layer is deposited. A parametric study on UiO-66-NH_2@GO nanohybrid concentration was conducted to verify if material detachment was influenced by nanohybrid loading (Fig. S8d); UiO-66-NH_2@GO nanohybrid was chosen as it shows higher detachment compared to ZIF-8@GO. This study reveals that the degree of detachment was higher for the membranes with greater concentration of nanohybrid. Besides, this is much more pronounced when the exceeds 500 $mg{\cdot}m^{-2}$. The motivation of adding the second layer is to stick both PDA layers together trapping the

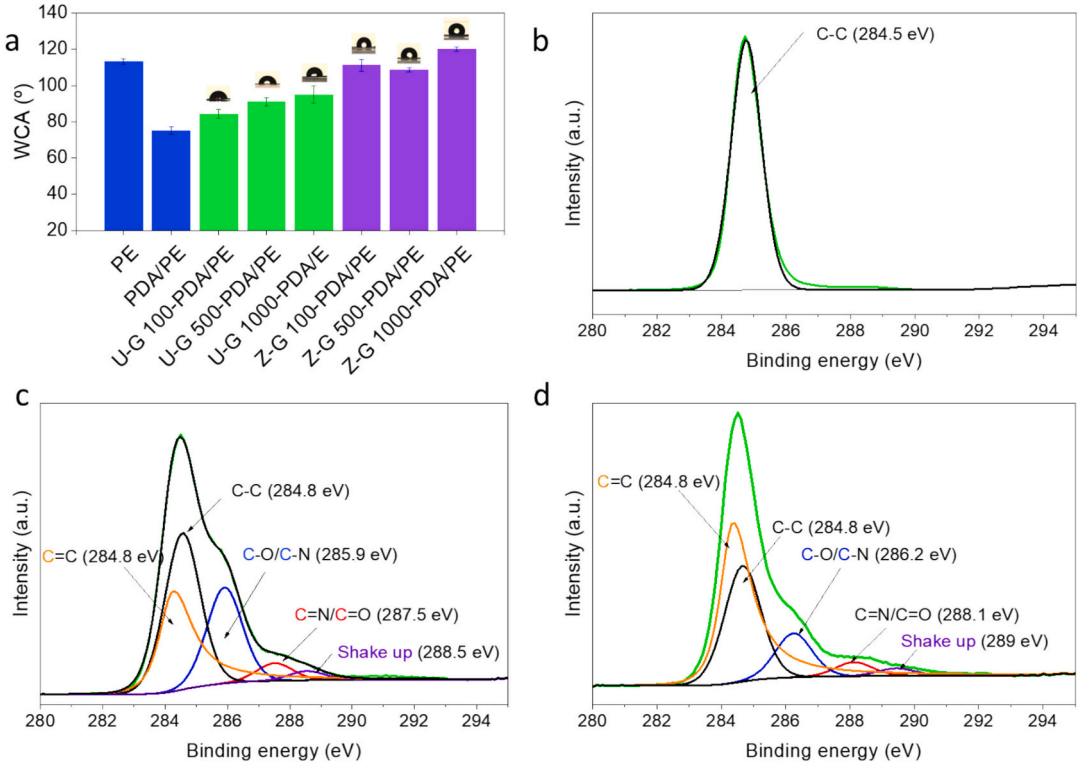

Fig. 6. WCA of prepared membranes (a) and C 1 s high resolution XPS spectra of bare PE polymer (b), PDA/PE (c), and Z-G 500-PDA/PE (d). Different colors represent the presence of the identified bonds, experimental signal (light green), and theoretical fitting (black).

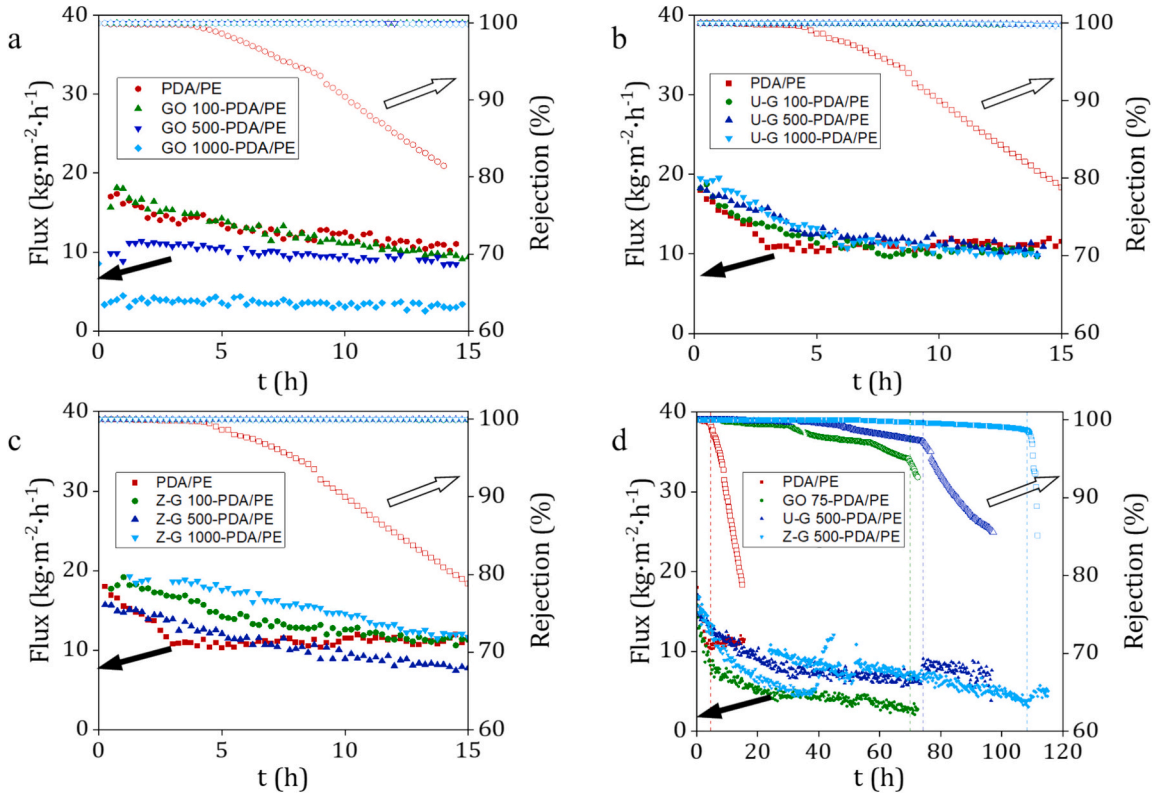

Fig. 7. AGMD performance of the synthesized membranes: GO PDA/PE (a), U-G PDA/PE (b) and ZIF-8@GO (c), and long-term stability study of selected membranes (d).

nanohybrids between. Then, if the loading of nanohybrid becomes too high, a significant area of the PDA is covered by the nanohybrids and the interactions between both PDA layers are limited, thus compromising the mechanical stability of the membranes. To sum up, the presence of the second layer of PDA is critical to ensure long-term stability, nanohybrid loading plays an important role in membrane stability, and ZIF-8@GO show minimal detachment even at loadings as high as 1000 $mg{\cdot}m^{-2}$.

3.3. AGMD experiments

All membranes were tested in AGMD configuration for water desalination. The feed stream contained 35 $g{\cdot}L^{-1}$ NaCl, 500 ppm HA and 420 ppm of $CaCl_2$, which was added to control the formation of HA coagulates [62] and investigate membrane performance in conditions of accelerated pore wetting, i.e. high concentration of foulants. The unmodified commercial PE membrane was tested as received and with two PDA coatings (PDA/PE) as a control membrane. Both PE and PDA/PE membranes show a similar behavior, where HA is quickly adsorbed to their surface and pore wetting occurred after 4.5 h (Fig. S9a). Those membranes containing GO (GO PDA/PE membranes) showed a decrease in water flux when increasing the nanohybrid loading (Fig. 7a), mainly due to the large average lateral size of GO flakes (up to 11 μm) that can partially block the pores of PE making the path of the water molecules more tortuous; GO 500-PDA/PE membrane shows a constant flux of about 10 $kg{\cdot}m^{-2}{\cdot}h^{-1}$ and GO 1000-PDA/PE membrane (double concentration of GO) shows half the flux (5 $kg{\cdot}m^{-2}{\cdot}h^{-1}$). However, the membrane at the lowest loading (GO 100-PDA/PE) behaves in a similar manner to the control membrane in terms of flux; i.e. flux starts at c.a. 17 $kg{\cdot}m^{-2}{\cdot}h^{-1}$ and gradually drops down to 11 $kg{\cdot}m^{-2}{\cdot}h^{-1}$. Interestingly, the salt rejection behavior is markedly different compared to the control PDA/PE membrane, which shows pore wetting at 4.5 h. Those membranes coated with GO showed a stable rejection above 99 % for the entire testing period (15 h). It is believed that electrostatic repulsion between carboxylic and phenolic groups of HA and negatively charged GO are responsible for maintaining rejection constant [63,64]. For the membranes coated with UiO-66-NH_2@GO (U-G PDA/PE) and ZIF-8@GO (Z-G PDA/PE), the flux does not fluctuate significantly when varying the loading of nanomaterial (Fig. 7b and c, respectively), distinctly to GO PDA/PE membranes (Fig. 7a). For all membranes containing the nanohybrids, water flux starts at c.a. 18 $kg{\cdot}m^{-2}{\cdot}h^{-1}$ and slowly decreases after 6–7 h of operation, reaching a plateau at c.a. 10–12 $kg{\cdot}m^{-2}{\cdot}h^{-1}$. Nevertheless, the membranes containing nanohybrids perform similarly to PE/PDA. This suggests that the additional porosity of the nanohybrid does not significantly affect water flux performance in the early stages of operation. Besides, both U-G PD/PE and Z-G PD/PE membranes achieved superior (>99 %) rejection over the entire tests (15 h). The lack of a clear trend between the flux and loading for the membranes containing nanohybrids —in contrast to GO membranes where the higher the loading, the the lower the flux— suggests a

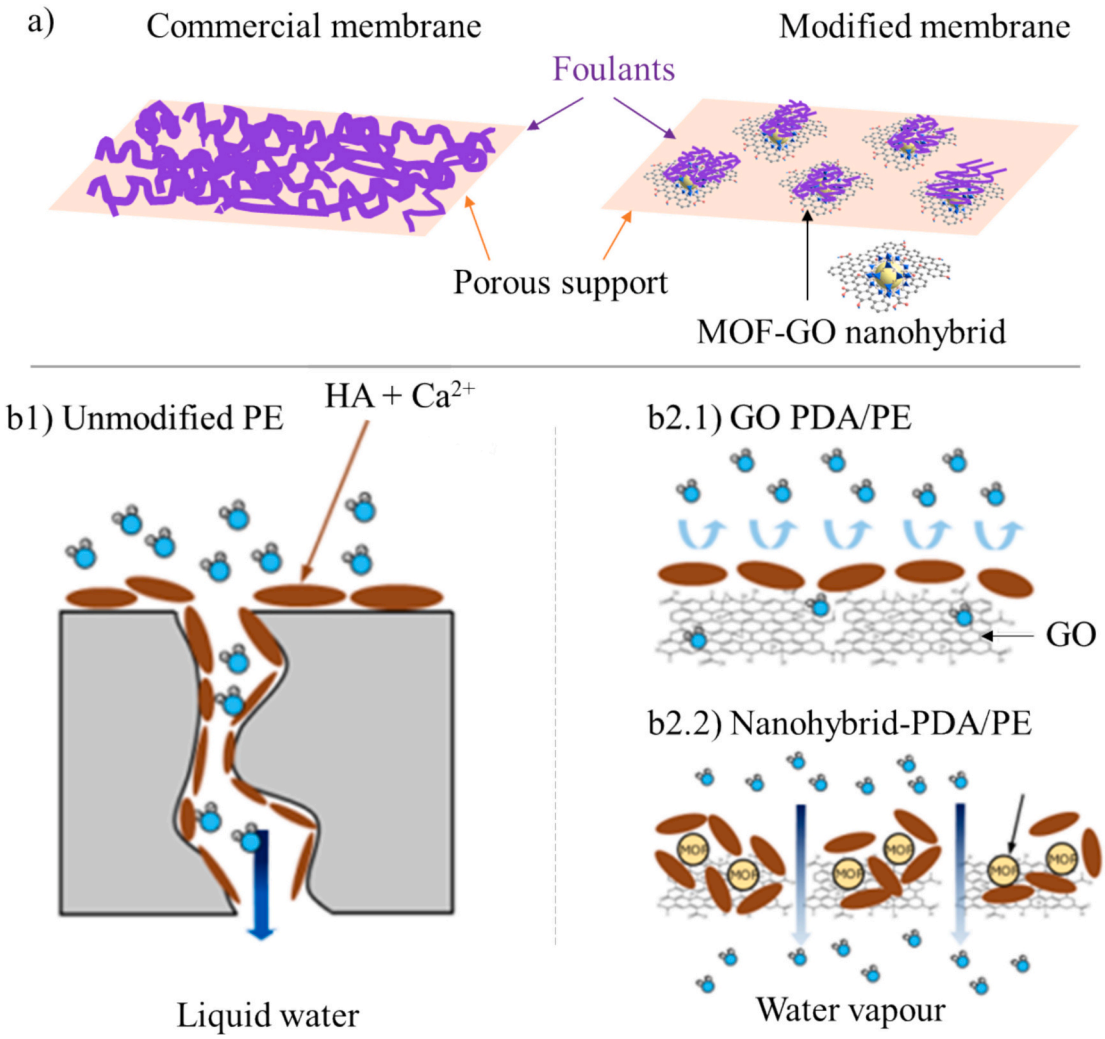

Fig. 8. Schematic diagram of fouling and pore wetting mechanisms at macroscopic (a) and at a molecular level (b), including (b1) bare PE membrane and modified membranes with GO (b2.1) or MOF@GO (b2.2) nanohybrids.

different interaction mechanism between HA molecules and the nanohybrids. Fig. S9b-d presents a comparative analysis of the flux and rejection for all loadings and membranes tested. As the loading increases, a decrease in flux is observed for membranes containing graphene oxide (GO), whereas those containing nanohybrids show a very similar flux regardless of the load used. This distinct behaviour is believed to be related to the strong HA adsorption properties of MOFs and will be thoroughly discussed later on (Fig. 8). Long-term performance (see Fig. 7d) was evaluated for U-G 500-PDA/PE and Z-G 500-PDA/PE membranes. This loading was selected for being the highest tested that did not suffer significant detachment from the membrane (see Fig. S8). The GO75 membrane was chosen as comparison since its GO concentration is the same as that in the U-G 500-PDA/PE membrane, according to calculated wt% (Fig. 3c). It can be seen that membranes containing the nanohybrids clearly outperform the membranes without them, including the membrane with GO. In all membranes, the flux followed a decrease at a pseudo-constant slow rate due to local organic fouling until complete deposition of HA molecules on the membrane surface occurred, where pore wetting is clearly noticeable. This caused a reduction in membrane surface tension, facilitating liquid passage through the membrane and wetting of the membrane pores. The membrane containing unmodified GO suffered a two step decline in rejection (at 30 and 57 h) before complete failure at 70 h. This phenomenon was delayed when the GO-based nanohybrids were used, achieving 74 and 109 h of sustained performance for UiO-66-NH_2@GO and ZIF-8@GO, respectively, due to the aforementioned differences in the fouling mechanisms associated with HA adsorption. Comparing the two MOFs, it can be seen that the ZIF-8 displays the highest fouling mitigation. This is believed to be related to its hydrophobic character, which has been imparted to the membrane as confirmed by the WCA measurements. It is well-established that enhanced hydrophobicity serves to prevent membrane wettability in porous membranes [8,65]. Given that fouling and pore wetting are surface-related mechanisms, it can be inferred that the adsorption properties of the surface functionalization are of considerable importance. HA adsorption experiments were conducted using UiO-66-NH_2@GO and ZIF-8@GO nanohybrids (Fig. S10). Both show a similar adsorption isotherms reaching a plateau at c.a. 60 and 55 $mg \cdot g^{-1}$ for UiO-66-NH_2@GO and ZIF-8@GO, respectively. Therefore, the enhanced stability of membranes containing ZIF-8@GO nanohybrids is attributed to the increased membrane hydrophobicity, rather than greater HA adsorption. Furthermore, *Z*-G PDA/PE membranes have shown lowest tendency to undergo detachment than U-G PDA/PE, which would also potentially contribute to extend its operation. It is important to reiterate that accelerated fouling conditions (c.a. 100 times the amount of HA in typical water) were used for the experiments. However, high loadings of MOF@GO nanohybrids as in this study may not be necessary, and it will depend on the amount of HA in the feed stream. This is particularly relevant when concerns to membrane stability, as it was proven that PDA/nanohybrid detachment is much more prone at higher loadings. Finally, Plots in Figs. S11–13 show the MD performance of different membrane specimens for the same membrane code, where high reproducibility can be observed.

Fig. 8a illustrates the proposed pore wetting mechanisms proposed to occur in the membranes reported in this study. When the unmodified PE or PDA/PE membranes are used, a hydrated foulant layer is formed on top (Fig. 8b1), resulting in pore wetting phenomenon. This leads to the formation of a hydrophilic bridge (mainly in the largest pores), and liquid water with dissolved salts starts to pass through the membrane and the rejection decreases at a pseudo constant rate (i.e. an abrupt loss in rejection at 4.5 h). In the GO PDA/PE membranes, a continuous layer of foulants is expected to grow parallel to the surface, creating additional mass transfer resistance (Fig. 8b2.1). This causes flux decline that gets more noticeable with the increase of GO loading (see Fig. 7a). For membranes containing both nanohybrids on their surface, it is believed that selective adsorption of foulant molecules takes place on the MOF nanoparticles due to their strong adsorption capacity. Thus, the existence of highly preferential adsorption sites on the surface results in the foulant layer growing perpendicular to the surface keeping a significant part of the membrane surface available for water molecules to pass through (Fig. 8b2.2). Therefore, membranes containing nanohybrids show lower flux decay and flux stabilization at larger values (e.g. 13 $kg \cdot m^{-2} \cdot h^{-1}$ for *Z*-G 1000-PDA/PE) compared to the GO-coated membranes (5 $kg \cdot m^{-2} \cdot h^{-1}$).

Membranes were also tested for simulated seawater separation with much lower concentration of humic acid. For that, a feed of 10 $mg \cdot L^{-1}$ HA, 420 $mg \cdot L^{-1}$ $CaCl_2$ and 35 $g \cdot L^{-1}$ NaCl was prepared. Results are depicted in Fig. 9.a and show the significative effect that feed concentration has in the long-term stability and operability; the ZG 500-PDA/PE membrane did not lose separation performance for 300 h, which is almost three times higher than the stability reached for accelerated fouling conditions (i.e. 500 $mg \cdot L^{-1}$ HA).

Performance recovery and reusability were also evaluated. For that, a fouled ZG 500-PDA/PE membrane (after 109 h of operation), was cleaned according to the following three-step procedure: i) it was rinsed thoroughly with DI water, ii) then it was submerged in an ultrasonic bath (10 min, 3 times) rinsing with DI water between cycles, and iii) the membrane was chemically cleaned with a 5 wt% HCl solution for 1 h. After that, the cleaned membrane was tested again under accelerated fouling conditions (i.e. high concentration of HA, of 500 $mg \cdot L^{-1}$). After 20 h of operation (Fig. 9b), membrane flux seemed completely steady and unaltered with rejection still >98 %. This confirms that the membrane can withstand acidic cleaning treatments.

Optical and SEM analysis of the membranes before and after AGMD operation (Fig. 10) were acquired to evaluate the fouling effect on the membrane morphology. Fig. 10a and d display images of a fresh *Z*-G 500-PDA/PE membrane, prior to undergoing testing. After MD, a thick hydrated HA deposition layer was formed on top of the surface (Fig. 10b and e). Fig. 10c and f show the same membrane after being rinsed with deionized water. It can be observed that the cake layer was removed but some salt crystals and HA foulants still remained attached to the membrane surface (Fig. 10e).

Membranes without the protective second PDA layer were tested in MD using a highly concentrated HA feed solution (500 mg/L). After 5 h of testing, during which some foulants were deposited but did not cover the entire surface, membranes were removed from the MD module and were analyzed by SEM-EDX to provide further insights into where the adsorption was taking place. Since the deposited fouling particles are composed of humic acid molecules coordinated with Ca^{2+} [66], the presence of these ions could be associated with more severe fouling at that specific location. SEM images and EDX spectra of samples Z-G 500-PDA/PE and U-G 500-PDA/PE are shown in Fig. S14, where element distribution on the nanohybrids and the polymer matrix is displayed. Ca was detected on top of the GO@MOF nanohybrids, for both ZIF-8@GO (Fig. S14.a) and UiO-66-NH_2@GO (Fig. S14.b), but not on the polymer matrix (Fig. S14.c-d). This suggests the aforementioned selective adsorption of fouling agents.

Lastly, a comparison with the literature on current membrane development in terms of anti-fouling and anti-wetting modifications is presented in Table 2. All these membranes are made of different polymers; typically, PVDF, Polypropylene (PP), Polysulfone (PSF), PE, PTFE. These materials are utilized in commercial membranes developed by various companies, including Aquastill and Tisch Scientific. However, they lack from for long-term operability, which has prompted efforts to develop new membranes and modify existing ones in order to achieve high performance and durability. Most of these efforts focused on superhydrophobization of the membrane surface (WCA > 150°), synthesis of omniphobic and Janus membranes, and incorporation of nanomaterials such as MOF or 2D materials. For instance, Zhang et al. [67] synthesized a superhydrophobic and oleophobic membrane immobilizing SiNPs on the PVDF support. Silica NPs was then fluorosilanized by a silane coupling agent with the aid of a PDA. WCA increased from 127 to 169° and membranes were tested for DCMD, with

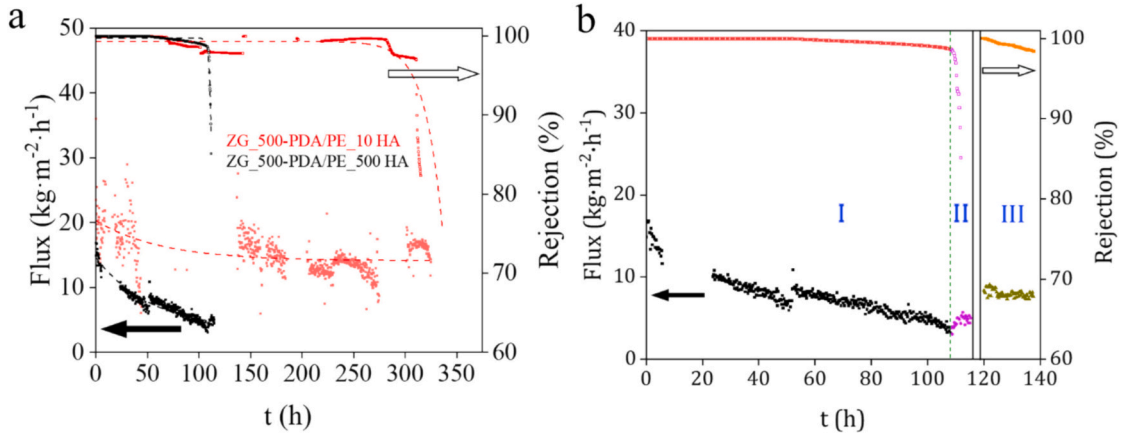

Fig. 9. Humic acid concentration effect on membrane separation capacities. ZG 500-PDA/PE in 10 mg·L^{-1} HA, 420 mg·L^{-1} $CaCl_2$ mg·L^{-1} and 35 g·L^{-1} NaCl (in red) and ZG 500-PDA/PE in 500 mg·L^{-1} HA, 420 mg·L^{-1} $CaCl_2$ mg·L^{-1} and 35 g·L^{-1} NaCl (in black) (a). Recycling and reusability of ZG 500-PDA/PE membrane. Figure is divided in 3 regions; I: Pre-pore wetting. II: pore wetting. III: after cleaning (b).

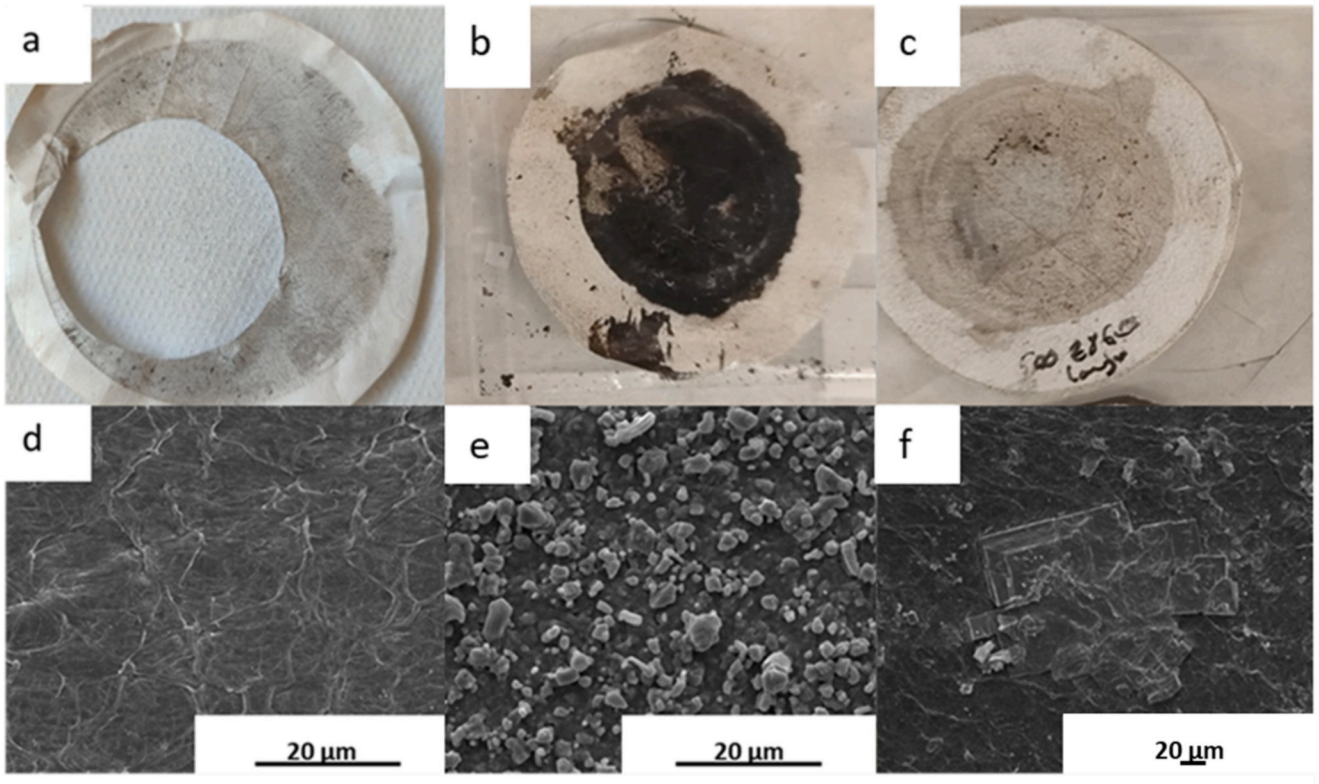

Fig. 10. Photographs (top) and SEM images (down) of Z-G 500-PDA/PE membranes: before use (a and d), after use (b and e), and rinsed with DI water after use (c and f).

a feed composed of NaCl, HA and $CaCl_2$, showing a stable permeate flux for 150 h. Hou et al. [68] also studied the effect of adding SiNPs on a PVDF substrate. In this case, they prepared PVDF-HFP/SiNPs flat-sheet hybrid membranes by electrospinning, getting enhanced in roughness and superhydrophobic membranes and achieving up to 240 h of stable flux for a NaCl feed solution. The superhydrophobic surface (WCA higher than 170°) accounts for the membrane durability. However, these fluorinated compounds are not only difficult to obtain, but also have a detrimental impact on the environment, particularly due to their high resistance to degradation and accumulation in water systems. Certain fluoro-compounds have also been linked to various health issues like cancer or thyroid problems. MXene, an emerging hydrophilic 2D nanomaterial, has attracted a lot of attention to prepare Janus membranes for MD. These materials have plenty of interesting qualities for this purpose: hydrophilicity, high thermal conductivity and mechanical stability. Yan et al. [69] modified a PVDF support using Polydimethylsiloxane (PDMS) to enhance wettability, and immobilized hydrophilic MXene to a PEI/PDA layer through hydrogen bonds. This leads to a Janus MXene membrane reaching up to 15 h of stable flux and salt rejection for a NaCl and sodium dodecyl sulfate (SDS) feed solution. MOFs and GO have also been investigated to improve flux and fouling resistance enhancement due to their high surface area, porosity and tunability [70]. Kebria et al. [71] synthesized a TFN with an ultrathin ZIF-8/chitosan layer coated on a PVDF support, which greatly improved

Table 2
Comparison and benchmarking of present's work-developed membranes in literature.

Polymer	Modification	Feed	Driving force	Configuration	Flux	Wetting resistance		Ref.
					R (%)	Before modification	After modification	
PVDF	Silica coating with fluorosilanization	35 g/L NaCl 50 ppm HA 1.26 g/L $CaCl_2$	50 °C	DCMD	37 $L{\cdot}m^{-2}{\cdot}h^{-1}$ 99.99 %	30 h	150 h	[67]
PVDF	PDMS coating plus MXene incorporation	0.4 mM SDS 15 g/L NaCl	68	DCMD	9.5–6 $L{\cdot}m^{-2}{\cdot}h^{-1}$ 99.99 %	5 h	> 15 h	[69]
PDA/ PEI	Si nanoparticles with a PVDF layer	0.5 mM NaCl 0.1 mM SDS 1 g/L mineral oil	40 °C	DCMD	19–16 $L{\cdot}m^{-2}{\cdot}h^{-1}$ 99.99 %	4 h	72 h	[72]
PVDF	Hydrophobization with PDANPs and PDMS	35 g/L NaCl 1.26 g/L $CaCl_2$	75 °C and 95 kPa vacuum	VMD	14–13 $L{\cdot}m^{-2}{\cdot}h^{-1}$ 99.99 %	6 h	> 25 h	[73]
PVDF	PVDF-HFP/Silica nanoparticles flat sheet hybrid	35 g/L NaCl	33 °C	DCMD	15 $L{\cdot}m^{-2}{\cdot}h^{-1}$ 99.99 %	240 h	Scaling removed	[68]
PES	PES superhydrophilic membranes were coated with PDMS and SiO_2	35 g/L NaCl 10 mg/L HA 1.47 g/L $CaCl_2{\cdot}2H_20$	40 °C	DCMD	12 $L{\cdot}m^{-2}{\cdot}h^{-1}$ 99.99 %	15 h	Fouling also removed	[74]
PES	Amphiphobization by dipcoating with SiNPS and coating with FDTES and PDMS	60 g/L NaCl 40 mg/L HA	40 °C	DCMD	16–13 $L{\cdot}m^{-2}{\cdot}h^{-1}$ 99.50 %	24 h	Fouling also removed	[75]
PVDF	Superhydrophobization with PFPE coating cured by UV	35 g/L NaCl 100 mg/L HA saturated $CaCO_3$	55 °C and 90 kPa vacuum	VMD	30–25 $L{\cdot}m^{-2}{\cdot}h^{-1}$ 99.99 %	8 h	> 25 h	[76]
PVDF	Addition of GO flakes, concentration optimization	35 g/L NaCl 150 ppm Triton X-100	55 °C	AGMD	9 $L{\cdot}m^{-2}{\cdot}h^{-1}$ 99.99 %	0.6 h	80 h	[21]
PE	Addition of UiO-66-NH_2 and ZIF-8@GO hybrids	35 g/L NaCl 500 mg/L HA 420 mg/L $CaCl_2$	68 °C	AGMD	17–11 $L{\cdot}m^{-2}{\cdot}h^{-1}$ 98.50 %	4.5 h	109 h	This work

AGMD performance. They experienced approximately 350 % water flux improvement with 99,5 % NaCl stable rejection for 15 h when tested with real seawater. Alberto et al. [21] conducted a similar study. The modified the surface of commercial PVDF membranes by adding GO embedded between two polydopamine layers that kept the 2D material in place. They reached up to 100 h of efficient separation when using a feed containing high concentration of a surfactant (Triton X-100), delaying pore wetting over 100 times as compared to bare support.

It is inherently challenging to establish a comparison between different studies, as the long-term performance is significantly influenced by the feed concentration and composition, which vary considerably between different works. However, it can be stated with certainty that the membranes prepared in this study, are capable of competing with those produced in previous studies in terms of long-term performance. This is due to the exploitation of both MOF and GO properties and the generation of "sacrificial" adsorption sites. Furthermore, our approach allows for the utilization of environmentally benign solvents and facilitates straightforward modifications to the nanohybrid coating concentration.

4. Conclusions

ZIF-8@GO and UiO-66-NH_2@GO nanohybrids were employed to modify the surface of a hydrophobic commercial polyethylene membrane. Both nanohybrids were deposited via vacuum filtration and embedded between two PDA layers, which has proved to be an excellent way of attaching these nanohybrids to the membrane for a load of 500 $mg{\cdot}m^{-2}$ or below. The formation of the PDA layers and nanohybrid deposition were confirmed by different characterization techniques, such as SEM, XPS, WCA, and AFM. Increased surface roughness, modified hydrophobicity, and adsorption properties were found to be critical in delaying fouling and pore wetting. A pore-wetting mitigation mechanism has been proposed where the addition of the nanohybrids results in selective fouling due to the interaction between nanohybrids and fouling agents. Nanohybrids containing ZIF-8 show better behavior in preventing fouling, pore wetting and detachment, which is attributed to its higher hydrophobic character. Membranes ZIF-8@GO 500 PDA/PE, reached up to 109 h of operability (compared to 4.5 h for bare PDA/PE membranes or 69 h for membranes containing unmodified GO) under accelerated aging conditions. In contrast, it is hypothesized that GO nanosheets cause the formation of a foulant layer resulting in partial blockage of pores at higher loadings, decreasing flux and stabilizing at lower values. The best performing membrane containing nanohybrids (i.e. *Z*-G 500-PDA/PE) improved membrane lifetime by 2300 % (4.5 to 109 h) and 58 % (69 to 109 h) as compared to PE and GO-PDA/PE, respectively.

CRediT authorship contribution statement

Andoni Moriones: Investigation, Methodology, Writing- Original draft preparation. **Lucía Cano-Herranz:** Investigation, Methodology. **Jose Miguel Luque-Alled:** Conceptualization, Methodology,

Investigation, Supervision, Writing- Reviewing and Editing. **Carlos Téllez:** Supervision, Writing- Reviewing and Editing,. **Patricia Gorgojo:** Conceptualization, Methodology, Supervision, Writing- Reviewing and Editing, Funding acquisition.

Declaration of competing interest

The authors declare that they have no known competing financial interests or personal relationships that could have appeared to influence the work reported in this paper.

Acknowledgements

Project TED2021-130557A-I00 funded by MCIN/AEI/10.13039/501100011033 and the European Union NextGenerationEU/PRTR. The authors would like to thank the University of Zaragoza for the use of the "Servicio General de Apoyo a la Investigación-SAI" and the use of instrumentation as well as the technical advice provided by the National Facility ELECMI ICTS, node "Laboratorio de Microscopias Avanzadas", at the "Universidad de Zaragoza". The Government of Aragon is also gratefully acknowledged for financing the T68_23R group. Grant CEX2023-001286-S funded by MICIU/AEI/10.13039/501100011033 is also acknowledged. J. M. Luque-Alled acknowledges the Spanish Ministerio de Universidades and the European Union-NextGenerationEU Fund for funding through the Margarita Salas and Juan de la Cierva programmes.

Appendix A. Supplementary data

Supplementary data to this article can be found online at https://doi.org/10.1016/j.desal.2025.118722.

Data availability

No data was used for the research described in the article.

References

[1] L. Wan, H.B. Wang, Control of urban river water pollution is studied based on SMS, Environ. Technol. Innov. 22 (2021), https://doi.org/10.1016/j.eti.2021.101468.
[2] UN-Warer., Summary Progress Update 2021 – SDG 6 – Water and Sanitation for All, 2021.
[3] V.G. Gude, N. Nirmalakhandan, S.G. Deng, Renewable and sustainable approaches for desalination, Renew. Sust. Energ. Rev. 14 (9) (2010) 2641–2654, https://doi.org/10.1016/j.rser.2010.06.008.
[4] V. Ranade, B. V., Industrial Wastewater Treatment, Recycling and Reuse, 2014.
[5] M. Elimelech, W.A. Phillip, The future of seawater desalination: Energy Technology, and the Environment, Science 333 (6043) (2011) 712–717, https://doi.org/10.1126/science.1200488.
[6] Y.D. Kim, K. Thu, S.H. Choi, Solar-assisted multi-stage vacuum membrane distillation system with heat recovery unit, Desalination 367 (2015) 161–171, https://doi.org/10.1016/j.desal.2015.04.003.
[7] Z.S. Tai, M.H.D. Othman, K.N. Koo, W. Mustapa, F. Kadirkhan, Membrane innovations to tackle challenges related to flux, energy efficiency and wetting in membrane distillation: a state-of-the-art review, Sustain. Mater. Technol. 39 (2024), https://doi.org/10.1016/j.susmat.2023.e00780.
[8] J.M. Luque-Alled, S. Leaper, A. Abdel-Karim, C. Skuse, P. Gorgojo, PVDF membranes containing alkyl and perfluoroalkyl-functionalized graphene nanosheets for improved membrane distillation, journal of environmental, Chem. Eng. 11 (3) (2023), https://doi.org/10.1016/j.jece.2023.109898.
[9] U.K. Kesieme, N. Milne, H. Aral, C.Y. Cheng, M. Duke, Economic analysis of desalination technologies in the context of carbon pricing, and opportunities for membrane distillation, Desalination 323 (2013) 66–74, https://doi.org/10.1016/j.desal.2013.03.033.
[10] E. Drioli, A. Ali, F. Macedonio, Membrane distillation: recent developments and perspectives, Desalination 356 (2015) 56–84, https://doi.org/10.1016/j.desal.2014.10.028.
[11] S. Al-Obaidani, E. Curcio, F. Macedonio, G. Di Profio, H. Ai-Hinai, E. Drioli, Potential of membrane distillation in seawater desalination: thermal efficiency, sensitivity study and cost estimation, J. Membr. Sci. 323 (1) (2008) 85–98, https://doi.org/10.1016/j.memsci.2008.06.006.
[12] A. Samadi, T.L. Ni, E. Fontananova, G. Tang, H. Shon, S.F. Zhao, Engineering antiwetting hydrophobic surfaces for membrane distillation: a review, Desalination 563 (2023), https://doi.org/10.1016/j.desal.2023.116722.
[13] A. Zarebska, D.R. Nieto, K.V. Christensen, B. Norddahl, Ammonia recovery from agricultural wastes by membrane distillation: fouling characterization and mechanism, Water Res. 56 (2014) 1–10, https://doi.org/10.1016/j.watres.2014.02.037.
[14] L. Fortunato, H. Elcik, B. Blankert, N. Ghaffour, J. Vrouwenvelder, Textile dye wastewater treatment by direct contact membrane distillation: membrane performance and detailed fouling analysis, J. Membr. Sci. 636 (2021), https://doi.org/10.1016/j.memsci.2021.119552.
[15] F.C.R. Costa, C.R. dos Santos, M.C.S. Amaral, Trace organic contaminants removal by membrane distillation: a review on mechanisms, performance, applications, and challenges, Chem. Eng. J. 464 (2023), https://doi.org/10.1016/j.cej.2023.142461.
[16] M. Gryta, Fouling in direct contact membrane distillation process, J. Membr. Sci. 325 (1) (2008) 383–394, https://doi.org/10.1016/j.memsci.2008.08.001.
[17] T. Horseman, Y.M. Yin, K.S.S. Christie, Z.X. Wang, T.Z. Tong, S.H. Lin, Wetting, scaling, and fouling in membrane distillation: state-of-the-art insights on fundamental mechanisms and mitigation strategies, Acs Es&T, Engineering 1 (1) (2021) 117–140, https://doi.org/10.1021/acsestengg.0c00025.
[18] D.M. Warsinger, J. Swarninathan, E. Guillen-Burrieza, H.A. Arafat, J.H. Lienhard, Scaling and fouling in membrane distillation for desalination applications: a review, Desalination 356 (2015) 294–313, https://doi.org/10.1016/j.desal.2014.06.031.
[19] S. Seraj, T. Mohammadi, M.A. Tofighy, Graphene-based membranes for membrane distillation applications: a review, journal of environmental, Chem. Eng. 10 (3) (2022), https://doi.org/10.1016/j.jece.2022.107974.
[20] S.S. Ray, H.S. Bakshi, R. Dangayach, R. Singh, C.K. Deb, M. Ganesapillai, S.S. Chen, M.K. Purkait, Recent developments in nanomaterials-modified membranes for improved membrane distillation performance, Membranes 10 (7) (2020) 29, https://doi.org/10.3390/membranes10070140.
[21] M. Alberto, C. Skuse, M. Tamaddondar, P. Gorgojo, Immobilized graphene oxide-based membranes for improved pore wetting resistance in membrane distillation, Desalination 537 (2022), https://doi.org/10.1016/j.desal.2022.115898.
[22] Kang-Jia Lu, Jian Zuo, Tai-Shung Chung, Novel PVDF membranes comprising n-butylamine functionalized graphene oxide for direct contact membrane distillation, J. Membr. Sci. ISSN: 0376-7388 539 (2017) 34–42, https://doi.org/10.1016/j.memsci.2017.05.064.
[23] J. Zahirifar, J. Karimi-Sabet, S.M.A. Moosavian, A. Hadi, P. Khadiv-Parsi, Fabrication of a novel octadecylamine functionalized graphene oxide/PVDF dual-layer flat sheet membrane for desalination via air gap membrane distillation, Desalination 428 (2018) 227–239, https://doi.org/10.1016/j.desal.2017.11.028.
[24] Y.C. Woo, L.D. Tijing, W.-G. Shim, J.-S. Choi, S.-H. Kim, T. He, E. Drioli, H.K. Shon, Water desalination using graphene-enhanced electrospun nanofiber membrane via air gap membrane distillation, J. Membr. Sci. 520 (2016) 99–110, https://doi.org/10.1016/j.memsci.2016.07.049.
[25] N. Hanikel, X.K. Pei, S. Chheda, H. Lyu, W. Jeong, J. Sauer, L. Gagliardi, O.M. Yaghi, Evolution of water structures in metal-organic frameworks for improved atmospheric water harvesting, Science 374(6566) (2021) 454-+. doi:https://doi.org/10.1126/science.abj0890.
[26] M.U. Shahid, T. Najam, M. Islam, A.M. Hassan, M.A. Assiri, A. Rauf, A.U. Rehman, S.S.A. Shah, M.A. Nazir, Engineering of metal organic framework (MOF) membrane for waste water treatment: synthesis, applications and future challenges, J. Water Process Eng. 57 (2024), https://doi.org/10.1016/j.jwpe.2023.104676.
[27] K.S. Park, Z. Ni, A.P. Cote, J.Y. Choi, R.D. Huang, F.J. Uribe-Romo, H.K. Chae, M. O'Keeffe, O.M. Yaghi, Exceptional chemical and thermal stability of zeolitic imidazolate frameworks, Proc. Natl. Acad. Sci. USA 103 (27) (2006) 10186–10191, https://doi.org/10.1073/pnas.0602439103.
[28] J. Winarta, B.H. Shan, S.M. McIntyre, L. Ye, C. Wang, J.C. Liu, B. Mu, A decade of UiO-66 research: a historic review of dynamic structure, synthesis mechanisms, and characterization techniques of an archetypal metal-organic framework, Cryst. Growth Des. 20 (2) (2020) 1347–1362, https://doi.org/10.1021/acs.cgd.9b00955.
[29] S. Salehi, M. Jahanshahi, M. Peyravi, Poly(vinylidene difluoride) membrane assisted by modified ZnO/ZIF nanoparticles for membrane distillation, Chem. Eng. Technol. 41 (10) (2018) 1994–2004, https://doi.org/10.1002/ceat.201700496.
[30] S. Dutta, R.F. de Luis, J. Goscianska, A. Demessence, R. Ettlinger, S. Wuttke, Metal–Organic Frameworks for Water Desalination, Advanced Functional Materials n/a(n/a) (2023) 2304790. doi:https://doi.org/10.1002/adfm.202304790.
[31] F. Li, L. Chen, Y. Wei, Z. Yin, K. Que, A novel UiO-66-NH2/graphene oxide composite thin membrane for retarding membrane wetting in membrane distillation, J. Ind. Eng. Chem. 123 (2023) 62–71, https://doi.org/10.1016/j.jiec.2023.03.022.
[32] Y. Mao, J. Xu, H. Chen, G. Liu, Z. Liu, L. Cheng, Y. Guo, G. Liu, W. Jin, Hydrophobic metal-organic framework@graphene oxide membrane with enhanced water transport for desalination, J. Membr. Sci. 669 (2023) 121324, https://doi.org/10.1016/j.memsci.2022.121324.
[33] S. Cao, T. Tang, C. Xi, Z. Chen, Fabricating magnetic GO/ZIF-8 nanocomposite for amphetamine adsorption from water: capability and mechanism, Chem. Eng. J. 422 (2021) 130096, https://doi.org/10.1016/j.cej.2021.130096.
[34] H. Ha, C.J. Ellison, Polymer/graphene oxide (GO) thermoset composites with GO as a crosslinker, Korean J. Chem. Eng. 35 (2) (2018) 303–317, https://doi.org/10.1007/s11814-017-0250-7.
[35] J. Wang, Y. Wang, Y. Zhang, A. Uliana, J. Zhu, J. Liu, B. Van der Bruggen, Zeolitic Imidazolate framework/graphene oxide hybrid Nanosheets functionalized thin film nanocomposite membrane for enhanced antimicrobial performance, ACS Appl. Mater. Interfaces 8 (38) (2016) 25508–25519, https://doi.org/10.1021/acsami.6b06992.

[36] S. Yang, Q. Zou, T. Wang, L. Zhang, Effects of GO and MOF@GO on the permeation and antifouling properties of cellulose acetate ultrafiltration membrane, J. Membr. Sci. 569 (2019) 48–59, https://doi.org/10.1016/j.memsci.2018.09.068.

[37] E.G. Masibi, T.A. Makhetha, R.M. Moutloali, E.G. Masibi, T.A. Makhetha, R.M. Moutloali, Effect of the Incorporation of ZIF-8@GO into the Thin-Film Membrane on Salt Rejection and BSA Fouling, Membranes 2022, Vol. 12, Page 436 12(4) (2022-04-17). doi:https://doi.org/10.3390/membranes12040436.

[38] R. Banerjee, A. Phan, B. Wang, C. Knobler, H. Furukawa, M. O'Keeffe, O.M. Yaghi, High-throughput synthesis of zeolitic imidazolate frameworks and application to CO2 capture, Science 319 (5865) (2008) 939–943, https://doi.org/10.1126/science.1152516.

[39] M. He, J. Yao, Q. Liu, K. Wang, F. Chen, H. Wang, Facile synthesis of zeolitic imidazolate framework-8 from a concentrated aqueous solution, Microporous Mesoporous Mater. 184 (2014) 55–60, https://doi.org/10.1016/j.micromeso.2013.10.003.

[40] Xiaomin Kang, Wanhao Cai, Song Zhang, Shuxun Cui, Xiaomin Kang, Wanhao Cai, Song Zhang, Shuxun Cui, Revealing the formation mechanism of insoluble polydopamine by using a simplified model system, Polym. Chem. 8 (5) (2017/01/31), https://doi.org/10.1039/C6PY02005D.

[41] L. Eykens, I. Hitsov, K. De Sitter, C. Dotremont, L. Pinoy, B. Van der Bruggen, Direct contact and air gap membrane distillation: differences and similarities between lab and pilot scale, Desalination 422 (2017) 91–100, https://doi.org/10.1016/j.desal.2017.08.018.

[42] M.S. El-Bourawi, Z. Ding, R. Ma, M. Khayet, A framework for better understanding membrane distillation separation process, J. Membr. Sci. 285 (1) (2006) 4–29, https://doi.org/10.1016/j.memsci.2006.08.002.

[43] Scaling and fouling in membrane distillation for desalination applications: a review, Desalination 356 (2015/01/15). doi:https://doi.org/10.1016/j.desal.2014.06.031.

[44] E. Curcio, X. Ji, G. Di Profio, A.O. Sulaiman, E. Fontananova, E. Drioli, Membrane distillation operated at high seawater concentration factors: role of the membrane on CaCO3 scaling in presence of humic acid, J. Membr. Sci. 346 (2) (2010) 263–269, https://doi.org/10.1016/j.memsci.2009.09.044.

[45] G.M. Marion, F.J. Millero, M.F. Camões, P. Spitzer, R. Feistel, C.T.A. Chen, pH of seawater, Mar. Chem. 126 (1) (2011) 89–96, https://doi.org/10.1016/j.marchem.2011.04.002.

[46] Ch. Baerlocher, Darren Brouwer, Bernd Marler and L.B. McCusker Database of Zeolite Structures. https://www.iza-structure.org/databases/.

[47] J. Abdi, M. Vossoughi, N.M. Mahmoodi, I. Alemzadeh, Synthesis of metal-organic framework hybrid nanocomposites based on GO and CNT with high adsorption capacity for dye removal, Chem. Eng. J. 326 (2017) 1145–1158, https://doi.org/10.1016/j.cej.2017.06.054.

[48] Koji Kida, Muneyuki Okita, Kosuke Fujita, Shunsuke Tanaka, Yoshikazu Miyake, Koji Kida, Muneyuki Okita, Kosuke Fujita, Shunsuke Tanaka, Yoshikazu Miyake, Formation of high crystalline ZIF-8 in an aqueous solution, CrystEngComm 15 (9) (2013/02/05), https://doi.org/10.1039/C2CE26847G.

[49] F. Farivar, P.L. Yap, R.U. Karunagaran, D. Losic, F. Farivar, P. Lay Yap, R.U. Karunagaran, D. Losic, Thermogravimetric Analysis (TGA) of Graphene Materials: Effect of Particle Size of Graphene, Graphene Oxide and Graphite on Thermal Parameters, C 2021, Vol. 7, Page 41 7(2) (2021-04-27). doi:https://doi.org/10.3390/c7020041.

[50] C.L. Luu, T.T.V. Nguyen, T. Nguyen, T.C. Hoang, C.L. Luu, T.T.V. Nguyen, T. Nguyen, T.C. Hoang, Synthesis, characterization and adsorption ability of UiO-66-NH2, Adv. Nat. Sci. Nanosci. Nanotechnol. 6(2) (2015-02-02). doi:https://doi.org/10.1088/2043-6262/6/2/025004.

[51] J.B. James, Y.S. Lin, Kinetics of ZIF-8 thermal decomposition in inert, oxidizing, and reducing environments, J. Phys. Chem. C 120 (26) (2016) 14015–14026, https://doi.org/10.1021/acs.jpcc.6b01208.

[52] M. Kandiah, M.H. Nilsen, S. Usseglio, S. Jakobsen, U. Olsbye, M. Tilset, C. Larabi, E.A. Quadrelli, F. Bonino, K.P. Lillerud, Synthesis and stability of tagged UiO-66 Zr-MOFs, Chem. Mater. 22 (24) (2010), https://doi.org/10.1021/cm102601v.

[53] Y. Cao, H. Zhang, F. Song, T. Huang, J. Ji, Q. Zhong, W. Chu, Q. Xu, Y. Cao, H. Zhang, F. Song, T. Huang, J. Ji, Q. Zhong, W. Chu, Q. Xu, UiO-66-NH2/GO Composite: Synthesis, Characterization and CO2 Adsorption Performance, Materials 2018, Vol. 11, Page 589 11(4) (2018-04-11). doi:https://doi.org/10.3390/ma11040589.

[54] Yitong Han, Min Liu, Keyan Li, Yi Zuo, Yingxu Wei, Shutao Xu, Guoliang Zhang, Chunshan Song, Zongchao Zhang, Xinwen Guo, Yitong Han, Min Liu, Keyan Li, Yi Zuo, Yingxu Wei, Shutao Xu, Guoliang Zhang, Chunshan Song, Zongchao Zhang, Xinwen Guo, Facile synthesis of morphology and size-controlled zirconium metal–organic framework UiO-66: the role of hydrofluoric acid in crystallization, CrystEngComm 17(33) (2015/08/10). doi:https://doi.org/10.1039/C5CE00729A.

[55] M. Wen, K. Mori, Y. Futamura, Y. Kuwahara, M. Navlani-García, T. An, H. Yamashita, M. Wen, K. Mori, Y. Futamura, Y. Kuwahara, M. Navlani-García, T. An, H. Yamashita, PdAg Nanoparticles within Core-Shell Structured Zeolitic Imidazolate Framework as a Dual Catalyst for Formic Acid-based Hydrogen Storage/Production, Scientific Reports 2019 9:1 9(1) (2019-10-30). doi:https://doi.org/10.1038/s41598-019-52133-5.

[56] Y. Cao, Y. Zhao, Z. Lv, F. Song, Q. Zhong, Preparation and enhanced CO2 adsorption capacity of UiO-66/graphene oxide composites, J. Ind. Eng. Chem. 27 (2015) 102–107, https://doi.org/10.1016/j.jiec.2014.12.021.

[57] S.A.E. Naser, K.O. Badmus, L. Khotseng, S.A.E. Naser, K.O. Badmus, L. Khotseng, Synthesis, Properties, and Applications of Metal Organic Frameworks Supported on Graphene Oxide, Coatings 2023, Vol. 13, Page 1456 13(8) (2023-08-18). doi:https://doi.org/10.3390/coatings13081456.

[58] M. Tanhaei, A.R. Mahjoub, V. Safarifard, Energy-efficient sonochemical approach for the preparation of nanohybrid composites from graphene oxide and metal-organic framework, Inorg. Chem. Commun. 102 (2019) 185–191, https://doi.org/10.1016/j.inoche.2019.02.024.

[59] H.Y. Erbil, C.E. Cansoy, Range of applicability of the Wenzel and Cassie−Baxter equations for Superhydrophobic surfaces†, Langmuir 25 (24) (July 27, 2009) https://doi.org/10.1021/la902098a.

[60] K. Maghsoudi, G. Momen, R. Jafari, The thermodynamic stability of the Cassie–Baxter regime determined by the geometric parameters of hierarchical superhydrophobic surfaces, Appl. Mater. Today 34 (2023) 101893, https://doi.org/10.1016/j.apmt.2023.101893.

[61] M. Samari, S. Zinadini, A.A. Zinatizadeh, M. Jafarzadeh, F. Gholami, M. Samari, S. Zinadini, A.A. Zinatizadeh, M. Jafarzadeh, F. Gholami, A new antifouling metal-organic framework based UF membrane for oil-water separation: A comparative study on the effect of MOF (UiO-66-NH2) ligand modification, Korean J. Chem. Eng. 2022 39:11 39(11) (2022-10-14). doi:https://doi.org/10.1007/s11814-022-1177-1.

[62] S. Srisurichan, R. Jiraratananon, A.G. Fane, Mass transfer mechanisms and transport resistances in direct contact membrane distillation process, J. Membr. Sci. 277 (1) (2006) 186–194, https://doi.org/10.1016/j.memsci.2005.10.028.

[63] M.J. A., L.K. Koopal, Kinetics of humic acid adsorption at solid-water interfaces, Environ. Sci. Technol. 33 (16) (July 14, 1999), https://doi.org/10.1021/es981236u.

[64] D.J. Johnson, N. Hilal, Can graphene and graphene oxide materials revolutionise desalination processes? Desalination 500 (2021) 114852 https://doi.org/10.1016/j.desal.2020.114852.

[65] M. Fouladivanda, J. Karimi-Sabet, F. Abbasi, M.A. Moosavian, Step-by-step improvement of mixed-matrix nanofiber membrane with functionalized graphene oxide for desalination via air-gap membrane distillation, Sep. Purif. Technol. 256 (2021), https://doi.org/10.1016/j.seppur.2020.117809.

[66] D. Zong, H. Xu, M. Ding, C. Yao, T. Lin, L. Gao, Effect of the cations on the humic acid induced membrane fouling in the membrane distillation process, DESALINATION 577 (2024), https://doi.org/10.1016/j.desal.2024.117398.

[67] W. Zhang, Y. Lu, J. Liu, X. Li, B. Li, S. Wang, Preparation of re-entrant and anti-fouling PVDF composite membrane with omniphobicity for membrane distillation, J. Membr. Sci. 595 (2020) 117563, https://doi.org/10.1016/j.memsci.2019.117563.

[68] D. Hou, D. Lin, C. Ding, D. Wang, J. Wang, Fabrication and characterization of electrospun superhydrophobic PVDF-HFP/SiNPs hybrid membrane for membrane distillation, Sep. Purif. Technol. 189 (2017) 82–89, https://doi.org/10.1016/j.seppur.2017.07.082.

[69] X. Yan, C. Yang, C. Ma, H. Tao, S. Cheng, L. Chen, G. Wang, X. Lin, C. Yao, A novel janus membrane modified by MXene for enhanced anti-fouling and anti-wetting in direct contact membrane distillation, Chemosphere 307 (2022) 136114, https://doi.org/10.1016/j.chemosphere.2022.136114.

[70] B.S. Lalia, E. Guillen, H.A. Arafat, R. Hashaikeh, Nanocrystalline cellulose reinforced PVDF-HFP membranes for membrane distillation application, Desalination 332 (1) (2014) 134–141, https://doi.org/10.1016/j.desal.2013.10.030.

[71] M.R.S. Kebria, A. Rahimpour, G. Bakeri, R. Abedini, Experimental and theoretical investigation of thin ZIF-8/chitosan coated layer on air gap membrane distillation performance of PVDF membrane, Desalination 450 (2019) 21–32, https://doi.org/10.1016/j.desal.2018.10.023.

[72] L. Meng, X. Chen, T. Cai, X. Tong, Z. Wang, Surface energy-induced anti-wetting and anti-fouling enhancement of Janus membrane for membrane distillation, Water Res. 263 (2024) 122176, https://doi.org/10.1016/j.watres.2024.122176.

[73] C. Li, W. Liu, J. Mao, L. Hu, Y. Yun, B. Li, Superhydrophobic PVDF membrane modified by dopamine self-polymerized nanoparticles for vacuum membrane distillation, Sep. Purif. Technol. 304 (2023) 122182, https://doi.org/10.1016/j.seppur.2022.122182.

[74] A.A. Khan, I.A. Khan, M.I. Siyal, C.-K. Lee, J.-O. Kim, Optimization of membrane modification using SiO2 for robust anti-fouling performance with calcium-humic acid feed in membrane distillation, Environ. Res. 170 (2019) 374–382, https://doi.org/10.1016/j.envres.2018.12.036.

[75] A.A. Khan, M.I. Siyal, C.-K. Lee, C. Park, J.-O. Kim, Hybrid organic-inorganic functionalized polyethersulfone membrane for hyper-saline feed with humic acid in direct contact membrane distillation, Sep. Purif. Technol. 210 (2019) 20–28, https://doi.org/10.1016/j.seppur.2018.07.087.

[76] J. Pan, F. Zhang, Z. Wang, S.-P. Sun, Z. Cui, W. Jin, O. Bamaga, H. Abulkhair, M. Albeirutty, E. Drioli, Enhanced anti-wetting and anti-fouling properties of composite PFPE/PVDF membrane in vacuum membrane distillation, Sep. Purif. Technol. 282 (2022) 120084, https://doi.org/10.1016/j.seppur.2021.120084.